

POLITECNICO DI TORINO

Master's Degree in Biomedical Engineering



**Politecnico
di Torino**

**Development of photocurable resins
for the fabrication of self-healing hydrogels
via Digital Light Processing 3D printing**

Supervisor:

Dott. Ignazio Roppolo

Candidate:

Riccardo Ariotti

A.Y. 2023/2024

ABSTRACT

Hydrogels represent a versatile class of biomaterials with unique properties that have gained significant interest across various fields. In particular, they have emerged as promising candidates for numerous biomedical applications thanks to their biocompatibility, tunable mechanical properties and ability to mimic biological tissues.

Self-healing hydrogels are biomaterials that can repair structural damage and recover their properties, similarly to human tissues. This characteristic makes these kinds of materials able to restore the morphology and mechanical properties after being damaged, thereby extending their lifespan and maintaining their structural integrity and functionality over time.

The aim of the work is to investigate a self-healing hydrogel based on a resin which can be 3D printed via Digital Light Processing (DLP). DLP consists in a layer-by-layer 3D printing technology based on the photopolymerization of liquid polymer, that allows rapid and precise fabrication of objects. The network of the above-mentioned hydrogel is composed of polyethylene glycol diacrylate (PEGDA), hydroxyethyl methacrylate (HEMA), dithiothreitol (DTT), and borax. The self-healing chemistry is mainly based on boronic ester bonds, a class of dynamic covalent bonds.

The experimental part consisted of studying the properties, including self-healing behaviour, of different formulations varying DTT-borax ratio and DTT-acrylates ratio, in order to select the optimal one in terms of mechanical properties recovery and 3D printing requirements. To do so, rheological and mechanical tests were performed. The results indicated that the printed hydrogel is able to recover its mechanical features even after multiple cycles of self-healing. Furthermore, the printing process was optimized, selecting parameters (such as time of exposure, light intensity, layer thickness) that best suited for a fast and controlled printing.

Index

1. Introduction.....	7
1.1 Hydrogels introduction.....	7
1.2 Hydrogels 3D printing background.....	9
1.3 Aim of the work.....	11
2. Intrinsic Self-Healing Mechanisms of Hydrogels.....	12
2.1 Dynamic covalent bonds.....	13
2.1.1 Imine bond.....	14
2.1.2 Metali-ligand interaction.....	15
2.1.3 Disulfide bond.....	16
2.1.4 Dies-Alder reaction.....	17
2.1.5 Acylhydrazone bond.....	18
2.1.6 Boronate ester bond.....	18
2.2 Non-covalent interactions.....	21
2.2.1 Electrostatic interaction.....	21
2.2.2 Hydrophobic interaction.....	22
2.2.3 Host-guest interaction.....	23
2.2.4 Hydrogen bond.....	24
3. 3D Printing.....	26
3.1 3D Printing overview.....	26
3.2 Photopolymerization.....	27
3.2.1 Photopolymerization mechanisms.....	28
3.2.2 Photocurable resin components.....	32
3.2.2.1 Monomers and oligomers.....	32

3.2.2.2 Photoinitiators.....	34
3.2.2.3 Dyes.....	34
3.2.2.4 Fillers.....	34
3.2.2.5 Radical scavengers.....	35
4. Vat Photopolymerization techniques.....	36
4.1 SLA: mechanism and features.....	36
4.2 CLIP: mechanism and features.....	37
4.3 DLP: mechanism and features.....	38
5. Materials and Methods.....	41
5.1 Materials.....	41
5.2 Formulations and preparation procedure.....	45
5.3 DLP 3D printer and sample preparation.....	46
5.4 Characterization methods.....	47
5.4.1. Preliminary tests.....	47
5.4.2 FTIR-ATR spectroscopy.....	48
5.4.3 Rheological testing.....	49
5.4.4 Mechanical testing.....	52
5.4.4.1 Tensile test.....	53
5.4.4.2 Compression test.....	55
5.4.5 Swelling test.....	56
6. Hydrogel Formulations Characterization: Results and Discussion.....	57
6.1 Preliminary tests.....	57
6.2 FTIR-ATR spectroscopy.....	60
6.3 Rheological analysis.....	64
6.3.1 Viscosity.....	65
6.3.2 Photorheology.....	66
6.4 Mechanical analysis.....	69

6.4.1 Tensile test.....	69
6.4.2 Compression test.....	74
6.5 Evaluation of printability and resolution in DLP 3D printing.....	75
6.6 Swelling test.....	81
6.7 Qualitative self-healing test.....	82
7. Conclusion.....	83

References

1. Introduction

1.1 Hydrogels Introduction

Hydrogels are three-dimensional networks composed of a hydrophilic polymeric structure, that can absorb large amounts of water. This property is shared with biological tissues, such as extracellular matrix. By designing and adjusting the composition of the polymer which composes the network, different mechanical properties can be achieved. In fact, hydrogels can be utilized as scaffolds for Tissue Engineering (TE) due to the possibility to easily regulate the physico-chemical properties [1].

For instance, a polylactideglycolic acid (PLGA) based hydrogel was used in a work with mesenchymal stem cells for cartilage regeneration to provide structural support and stimulate repair. The authors findings showed that in this engineered cartilage, the PLGA 3D structure also supported the differentiation of progenitor cells and demonstrated successful induction of *in-vivo* chondrogenesis [2].

Boucard et al. reported the successful use of chitosan-based hydrogel for skin regeneration following third-degree burns. Here, results showed that chitosan materials were well tolerated and promoted good tissue regeneration [3].

Because of this versatility, hydrogels have received significant attention in the field of biomedicine, in particular in TE and biosensors research [4].

Their properties can be tuned in response to various stimuli such as temperature and pH, depending on their physical and chemical properties. Several approaches and strategies can be exploited to produce hydrogels, which need to be chosen according to the capabilities and properties one wants to obtain from the final product. To develop biocompatible hydrogels, natural polymers such as gelatin, cellulose or dextran are often used due to their biologically recognizable moieties and biodegradability. However, these hydrogels are characterized by worse mechanical performances compared to the ones made of synthetic polymers, which, on the contrary, do not possess bioactive properties. To achieve a good mechanical behaviour while maintaining the capability to be biocompatible, some synthetic polymers structures can be modified to yield tailored degradability and functionality [5].

To increase biological and mechanical properties of these 3D polymeric networks, natural and synthetic hydrogels can be combined; Chen et al. synthesized a hybrid PLGA-based hydrogel and

prepared microsponges of collagen in the pores of PLGA. This 3D scaffold was used for *in-vitro* and *in-vivo* testing TE of bovine articular cartilage and demonstrated to be suited for chondrocytes cell adhesion and proliferation. The environment was appropriate for cell differentiation and allowed homogeneous cell distribution in the network. The PLGA porous 3D structure provided good mechanical strength and well defined the shape of the engineered tissue [6].

Poly(lactic acid) (PLA), poly(glycolic acid) (PGA), poly (N-isopropylacrylamide- co-methacrylic acid) (pNIPAAm) or poly(ethylene glycol) (PEG) and its derivatives are commonly employed polymers in preparing hydrogels. For example, pH- and thermo-responsive hydrogel systems for drug delivery were applied in cardiovascular treatments for local delivery of thrombolytic and antithrombotic agents using pNIPAAm-based hydrogels [7].

Moreover, a composite thermo-sensitive hydrogel made of pNIPAAm and poly(ethylene glycol) diacrylate (PEGDA) was developed and used in ocular drug delivery for delivering of proteins like immunoglobulin G (IgG). The authors established that this hydrogel was non-toxic, and the copolymer made of pNIPAAm and PEGDA was biocompatible [8].

In this context, another characteristic that hydrogels may possess and could make these materials similar to biological tissues is self-healing. Self-healing is a term used to describe the property of a class of materials that can recover from damages restoring the morphology and the mechanical properties, entirely or partially. This feature is important in biomedical applications such as TE scaffolds and implantable devices [9].

In fact, the implementation of self-healing properties into hydrogels enhances their longevity and durability, making them more reliable, cost-effective, and sustainable materials, reducing the need for frequent repairs and replacements. These abilities provide a possible solution to the degradation lead by environmental stresses such as mechanical stresses, chemical agents, or other conditions. In this way, it is ensured that the devices maintain their functionality and integrity over time within the body. With this in mind, hydrogels designed with the intrinsic ability to self-repair when exposed to destructive factors can serve as candidate biomaterials to address issues in tissue engineering and improve mechanical stability and durability in *in-vivo* bio-implants. Also, they can be manufactured to be robust, shear-thinning, or cell-adaptable, making them suitable for a broad range of applications including soft robots and drug delivery [10].

Self-healing hydrogels can be designed according to their intended application and can be synthesized via different chemistries and self-healing mechanisms, often based on physical cross-

linking and dynamic covalent bonds (Figure 1) [11]. This aspect will be discussed in detail in the next chapter.

It is important to adjust the doses of the components in order to obtain a polymer network that has the characteristics such that the intent is achieved. Therefore, it is necessary to adapt the hydrogel production and development process according to the needs of the case.

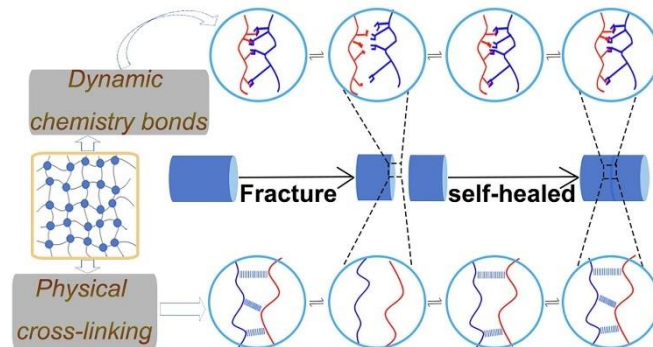


Figure 1. Self-healing mechanisms exploiting dynamic chemistry bonds and physical cross-linking.

1.2 Hydrogels 3D printing background

Despite the outstanding properties that hydrogels may have, one of the biggest issues with this kind of material is their shaping. Due to the low mechanical properties and their texture, hydrogels cannot be processed by tooling. Consequently, the most exploited technique for giving specific shapes are extrusion and molding.

In the last years, 3D printing technologies, or additive manufacturing (AM), have emerged as a powerful technique for hydrogel's production process. 3D printing allows the creation of complex structures with high precision. The combination of 3D printing technology with hydrogels opens up new possibilities in the biomedical field and expands the boundaries of materials science in general. The rapid advancement of research in developing biomaterial inks and bioinks for 3D printing reflects the feasibility of hydrogels [12].

Stimuli responsive hydrogels (SRH) have gained interest due to their ability to change their shape and mechanical properties in response to environmental stimuli. Through 3D printing of SRH, it is possible to create on-demand dynamically controllable shapes maintaining the control over other properties such as self-repair and multi-functionality. The stimuli for which hydrogels can be printed in a versatile way are various: pH, humidity, heat, light, magnetic and electric field and others. For

example, a magneto-responsive hydrogel was developed by Siminska-Stann and colleagues. They printed through multi-material printing a polyacrylic acid (PAA) structure in which they dispersed magnetic nanoparticles (MNPs). Calcium ions allowed the interaction and cross-linking between PAA and MNPs forming the hydrogel structure. Various MNPs patterns were created and the spatially anisotropy was achieved and confirmed in response under magnetic fields [13].

Various techniques are part of the 3D printing field, and each has its own strengths and limitations. Usually, they are divided according to their printing mechanism. Examples of these printing methods are the ones based on extrusion printing, laser printing, inkjet printing and photopolymerization-based techniques.

Amongst all these techniques, the ones that exploit Vat Photopolymerization (VPP) are well indicated for the purpose of printing complex architectures made of soft materials like hydrogels with high fabrication accuracy. Stereolithography (SLA), Digital Light Processing (DLP) and Continuous Liquid Interface Production (CLIP) are examples that fall into this category. One of the most interesting is DLP, which allows for resolutions down to 25 microns and reduced printing times. Through DLP, the photocurable resin is put in a vat. The photon source irradiates from the bottom of the resin vat the entire specific area that needs to be polymerized for each layer. The building platform on which the layers attach is dipped into the resin from above. With this technique, every point of each layer is cured simultaneously on the printing platform. The cured layers are not in direct contact with air, so oxygen inhibition phenomenon is limited, making the polymerization process more controlled and efficient. Moreover, the uncured resin can be reused, making this technology sustainable in terms of material consumption [14] [15].

For example, through DLP Chuhan et al. Were able to print a porous pNIPAAm and polypyrrole (PPy) based network capable of conducting electricity. The printed hydrogel was characterized by good pressure sensitivity and may be used as a piezo resistive sensor. In this work, through DLP technology the researchers were able to achieve good material shaping and conductivity [16].

Furthermore, Caprioli et al. were able to print via DLP a self-healing hydrogel made of poly (vinyl alcohol) (PVA), acrylic acid (AAc) and PEGDA. PEGDA played successfully its role as cross-linker during the printing phase, enabling the creation of an interpenetrated network in which reversible physical bonds and non-reversible chemical bonds were simultaneously present. Here, the physical network imparted self-healing ability to the hydrogel while the chemical cross-linked network conferred structural mechanical stability. Regarding the printed objects geometrical features, clean and sharp

edges, straight elements and smooth surfaces were achieved. Also, rounded geometries based on rotational symmetry and self-standing segments, that normally require additional support materials, were obtained without the need of any support [17].

1.3 Aim of the work

The purpose of the work is to study how, by varying the quantities of certain resin's components, self-healing efficiency and mechanical properties consequently vary, as well as the printing requirements. In those terms, we want to identify the optimal formulation. The synthesized resin is made of polyethylene glycol diacrylate (PEGDA), hydroxyethyl methacrylate (HEMA), dithiothreitol (DTT), and borax. Phosphate-buffered saline (PBS), photoinitiator (PI) and radical scavenger are also present. Self-healing is given by the ability of borax to form reversible inter-chain bridges via boronic ester bonds with DTT's exposed hydroxyl groups. The first set of formulations was produced varying the DTT-borax ratio in order to study its effect on the hydrogel's self-repair abilities. Subsequently, another set was produced varying the DTT-acrylates ratio, in order to investigate the mechanical properties such as stiffness or elastic modulus. The choice of the optimal formulation was made taking into account mechanical recovery features after break, self-healing efficiency and DLP printing requirements. To assess all these features, rheological, spectroscopic and mechanical tests were conducted.

In the following chapters, different intrinsic self-healing mechanisms are discussed, focusing on the boronic-ester dynamic covalent bond chemistry. Then, different photopolymerization processes are explained, with a focus on vat photopolymerization techniques. Additionally, DLP technology in hydrogel 3D printing is described, highlighting its strengths and limitations compared to other 3D printing techniques.

The last chapters deal with materials, methods and the results of the experimental work. The results will be discussed presenting the data obtained through the conducted tests.

2. Intrinsic Self-healing Mechanisms of Hydrogels

As mentioned, self-healing materials are a class of materials that exhibit the ability to restore themselves and recover their functionalities using resources available in the material [18].

This functions recovery is similar to the healing of the organism tissues. Self-healing hydrogels can be prepared with similar healing abilities due to the wide range of materials and different chemistries that can be exploited [10].

Moreover, extracellular matrix (ECM) -like features such as water retention and porous structure can be achieved. In this optic, self-healing hydrogels can have desirable biocompatibility and mechanical properties, enabling their application as structural biomaterials in the tissue engineering field [19].

Generally speaking, self-healing mechanisms can be divided into two main classes: intrinsic and extrinsic. Intrinsic mechanism relies on the ability of functional groups to re-establish bonds between surfaces, facilitating the restoration of structural integrity after damage. Extrinsic mechanism involves the presence in the network of reservoirs which contain unreacted monomers. These self-healing agents act when damage occurs in order to fill the cracks and recover mechanical stability locally [17].

Consequently, hydrogel materials based on intrinsic self-healing chemistries rely on their ability to break and reform bonds and interactions without the effect of a healing agent. The restoration of the material is accomplished thanks to the reversible linkages that can reform across the damaged surfaces. The restoration of these bonds leads to the healing of the material's structure, recovering entirely or partially its mechanical properties. Since self-healing is enabled by the functionalities embedded in the polymeric network, for these kinds of hydrogels it is possible to self-repair even after multiple healing cycles.

In developing self-healing hydrogels, the design and the self-healing mechanisms which can be chosen are various. In general, the two main self-healing mechanisms in hydrogels are related to dynamic covalent bonds (chemical crosslinking) and non-covalent interactions (physical crosslinking). Since non-covalent bonding is characterized by weak intermolecular forces, it is less strong compared with covalent bonding, but usually is more paid and not triggered by external stimuli. Commonly, dynamic covalent bonds exhibit stronger but slower dynamic equilibriums compared with non-covalent interactions, which show weak but rapid dynamic equilibriums.

Furthermore, those can be controlled by the application of certain conditions, such as light irradiation, temperature, and pH [20].

In *Figure 2*, intrinsic mechanisms for various self-healing hydrogels are depicted.

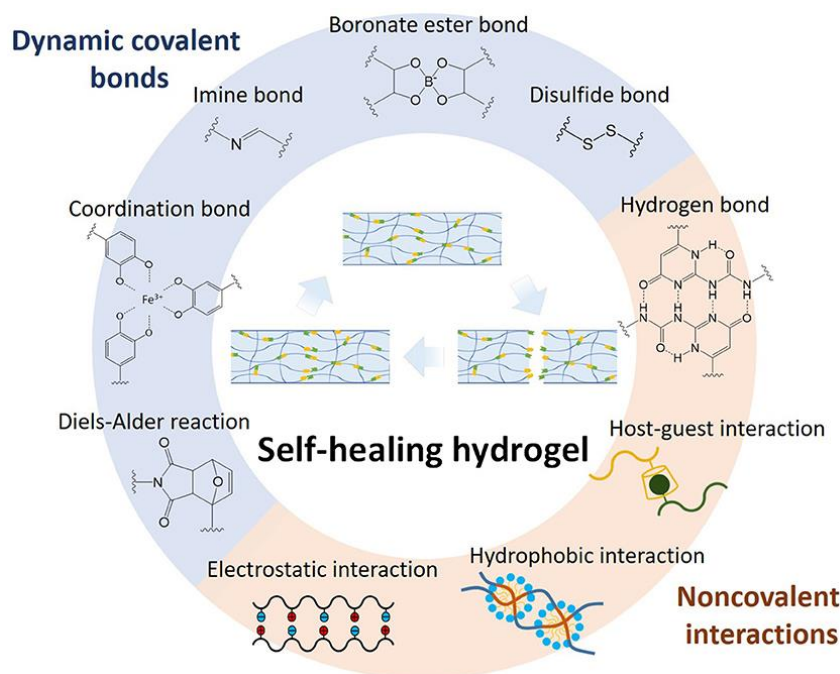


Figure 2. Chemistries and mechanisms for various self-healing hydrogel formulations.

2.1 Dynamic covalent bonds

The hydrogels based on dynamic covalent bond chemistry are capable to self-repair their structure due to the reversible nature of the covalent bonds involved in the network. These bonds can break and reform autonomously after damage. The reversible assembling and disassembling of components occur simultaneously and continuously in the whole system, finding an equilibrium. The efficiency of the self-healing process depends on the mobility of the polymer chains and the availability of reactive functional groups. The reversibility of the cross-linking points in polymers can be reached mainly in three different ways [21].

The first, consists in implementing functional groups to a linear copolymer backbone (*Figure 3a*) Secondly, the incorporation of reversible bonds can be made in a linear polymer main chain (*Figure 3b*). Here, if the bonds break and so the overall polymeric network, the mechanical properties will drop down. The third system exploits structures composed of bifunctional group molecules and elements with multiple binding sites. Here, reversible networks can form without the need of a permanent copolymer backbone (*Figure 3c*). Also, if damage occurs, the equilibrium can be shifted

toward debonding, increasing the chain mobility and allowing restoration of the damage sites through the re-establishment of the bonds [21].

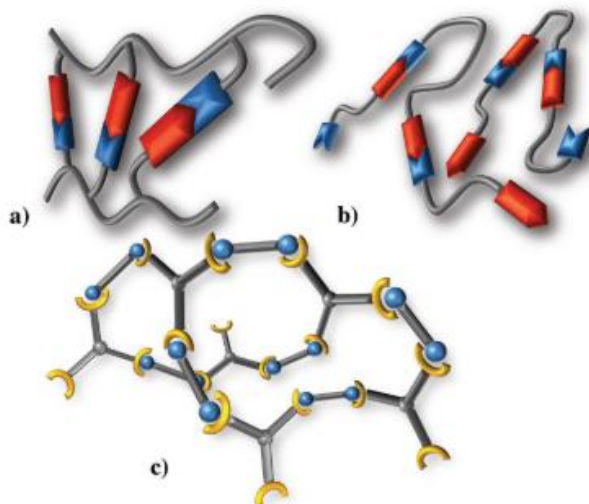


Figure 3. Schematic representation of the three concepts for reversible covalent polymer formation: a) Reversible bonds in the main chain, b) side chain, and c) network with multifunctional linker [21].

Hydrogel matrices that exploit these cited chemistries could exhibit some properties like pH-, thermo- and redox- responsiveness according to the nature of covalent bonds. There are various strategies that can be used to synthesize such hydrogels, here are briefly described the ones related to imine bond, metal-ligand interaction, disulfide bond, acylhydrazone bond, Diels-Alder reaction, boronate ester bond. The chemistry of the synthesized hydrogel in the experimental part of this work is based on the dynamic covalent boronate ester bonds. Therefore, more details about this class of reversible bonds will be provided and examples will be reported.

2.1.1 Imine bond

In the context of hydrogels, imine bonds, also known as Schiff bases, are typically formed by the reaction between aldehyde or ketone groups and amine groups. The general reaction (Figure 4), involves the nucleophilic attack of the amine on the carbonyl carbon, followed by the elimination of water, resulting in the formation of an imine. The reaction can take place under mild conditions. These dynamic covalent bonds can reversibly form and break in response to environmental changes such as pH, temperature, or the presence of certain chemicals. When the hydrogel is damaged, the

imine bonds break, but new ones can form if free amines and aldehyde groups are close, restoring the hydrogel integrity and enhancing its durability.

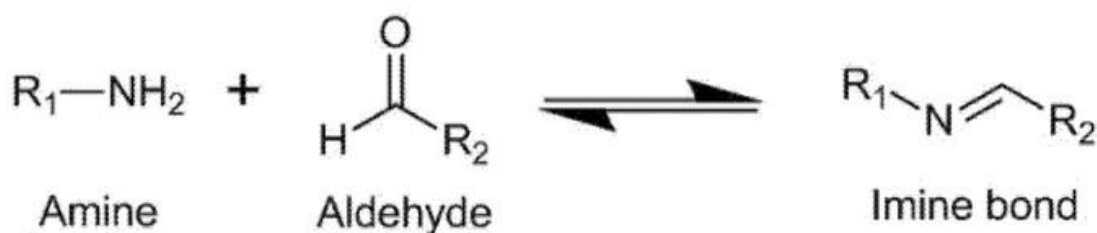


Figure 4. Imine bond formation's reaction.

Basu et al. have developed a nanocomposite DNA-based hydrogel crosslinked with oxidized alginate (OA) via the formation of reversible imine linkages. This hydrogel was produced to perform a sustained delivery of simvastatin, a small molecule. The results showed that the formulation exhibited self-healing due to the presence of reversible imine bonds formed between the amine groups of the DNA nucleotides and the aldehyde groups of OA. To confirm the successful formation of these covalent bonds rheological tests are presented. Varying OA concentrations, different formulations were considered. The test's results confirm changes in viscosity and G' values; as expected, the one with a higher concentration of OA, and so more imine bonds, result having higher values of G' and viscosity compared to the ones with low concentration of OA. The self-healing behaviour of the gels has been observed by monitoring the change in G' values while subjecting them to alternating high and low strains. Formulations where the presence of imine bonds is higher have showed higher G' recovery percentages, thus they addressed this result to the presence of reversible imine bonds performing self-healing [22].

2.1.2 Metal-ligand interaction

Also known as coordinate covalent bonds, this is another type of mechanism used in the design of self-healing hydrogels. These bonds form between organic ligands and metal ions, providing a reversible and dynamic crosslinking, and can be either part of the polymer backbone or incorporated as pendant groups. Common ligands used in self-healing hydrogels include carboxylates, and amines, which can form complexes with metal ions such as Zn^{2+} , Ca^{2+} , Cu^{2+} and Fe^{3+} . The bond formation mechanism is fundamentally achieved due to the metal ion's ability to accept electron pairs from ligands. The reaction is similar to an acid/base reaction. In *Figure 5* a reaction between four

molecules of ammonia and Cu^{2+} is reported. The ligands, acting as Lewis bases, donate their electron pairs to the empty or partially filled d orbitals of metal ions (Lewis acids).

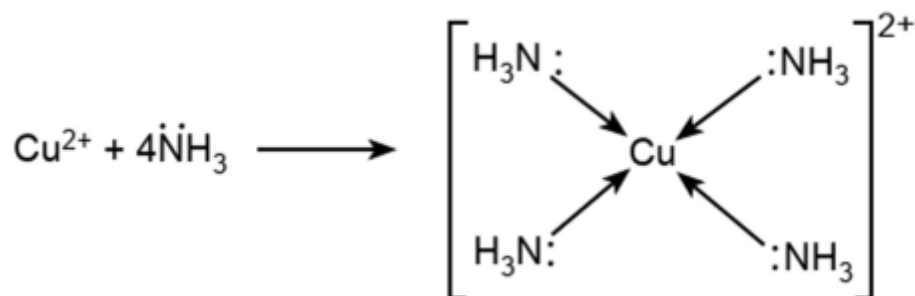


Figure 5. Metal-ligand interaction between ammonia and Cu^{2+} .

This interaction can be implemented to prepare self-healing hydrogels. Zhang et al. reported an injectable self-healing hydrogel in which hydrogen bonds and metal-ligand bonds simultaneous effect provide good self-repair ability. Gelatin molecule chains were modified introducing Urea pyrimidinone (UPy), a molecule that exposes carboxyl groups, and Fe^{3+} ions were added. The results from the conducted rheological tests revealed that the coordination between Fe^{3+} and $-\text{COOH}$ accounted for strength and partial self-healing behaviour of the prepared gelatin- Fe^{3+} -UPy hydrogel, while the introduction of UPy moieties further improved the self-healing property [23].

2.1.3 Disulfide bond

Disulfide bonds are a type of dynamic covalent bond that can significantly contribute to the self-healing properties of hydrogels. These bonds can form through the oxidation and can break through the reduction of two thiol ($-\text{SH}$) groups (Figure 6). The disulfide bonds are mainly used to prepare self-healing hydrogels from [synthetic polymers](#). For biopolymer-based hydrogels, the chemical modifications are required to provide biopolymers with the functional groups for these reactions.

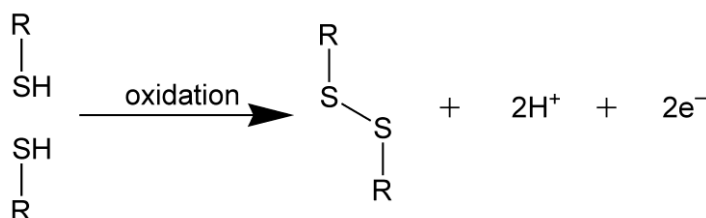


Figure 6. Schematic of a disulfide bond formation.

In Chen et al. work an injectable, self-healing coordinative hydrogel with antibacterial properties was prepared via cross-linking of multi-arm thiolated polyethylene glycol (SH-PEG) with silver nitrate (AgNO_3). The bonds involved in the formation of the network were disulfide bonds and coordination

S-Ag-S bonds. This hydrogel showed good self-healing and injectability properties. Other than that, the presence of Ag ions gives the hydrogel antibacterial properties, making it particularly appealing for skin wound repair [24].

2.1.4 Dies-Alder reaction

The Diels–Alder reaction is a cycloaddition reaction between a conjugated diene and a dienophile that forms a six-membered ring (*Figure 7*). It is a highly specific and efficient reaction; it proceeds under mild conditions. Given this, it's useful in the synthesis and design of hydrogels. Other advantages are the fast synthesis reaction and the thermal reversibility under physiological conditions.

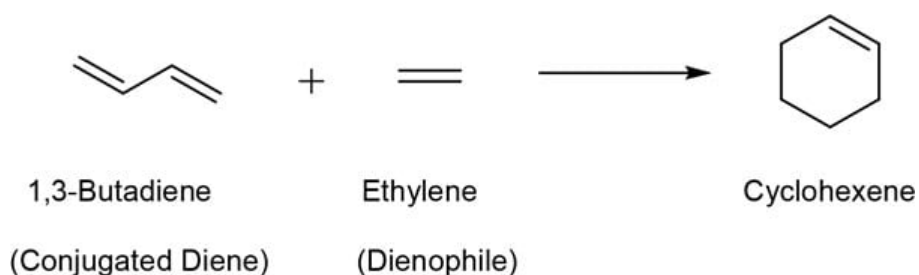


Figure 7. Example of a Dies-Alder reaction between 1,3-butadiene and ethylene.

The dynamic nature of the Dies-Aalder reactions allows the hydrogel to break and reform cross-links, enabling self-healing.

Wei et al. prepared a self-healing hydrogel Diels-Alder reaction between monomers fulvene-modified dextran and dichloromaleic-acid-modified poly (ethylene glycol) at physiological conditions. Self-healing after mechanical ruptures was rated positively thanks to the dynamic restructuring given by the reversible Dies-Alder linkages. Rheology recovery tests were conducted as well. Performing continuous step strain measurements, they found that under a 1.0% strain the hydrogel was solid-like, and at 1000% strain the hydrogel was fluidlike. After re-setting the strain at 1.0% and repeating this strain variations, the hydrogel recovered its G' and G'' initial values. Thus, this hydrogel demonstrated a fast recovery of internal networks when subjected to large strain variations [25].

2.1.5 Acylhydrazone bond

These bonds are usually formed via condensation reaction between hydrazine and ketones or aldehydes. In *Figure 8*, an example of this reaction is reported. The reaction can be performed at room temperature, and since dynamic covalent bonds are established, it can be exploited to prepare self-healing hydrogels.

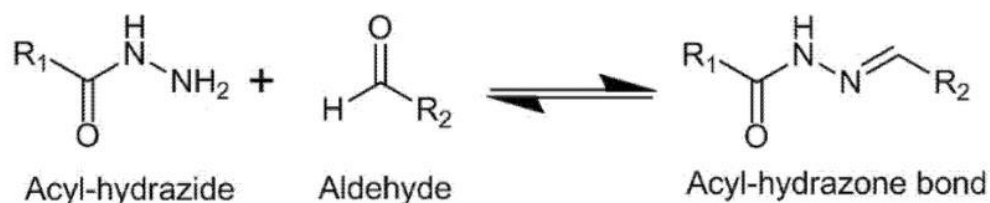


Figure 8. Example of acylhydrazone bond formation reaction.

Chang et al. prepared a self-healable hydrogel through acylhydrazone formation. The hydrogel is composed of N-isopropylacrylamide and acylhydrazine P(NIPAM-co-AH) cross-linked by PEO dialdehyde. The formation of the polymer network didn't need to be catalysed by additives. Here, self-healing is activated through the excess of acylhydrazine that activates the acylhydrazone exchange. Hydrogels healed for 24 hours didn't break at the cut line when stretched [26].

2.1.6 Boronate ester bond

Boronate ester bonds represent a class of dynamic covalent chemistry, through which responsive materials can be synthesized due to the bonds' ability of rearranging by breaking and reforming. To prepare gels that have good structural integrity and the ability to self-heal, permanent crosslinks can be achieved together with dynamic bonds such as boronate esters (*Figure 9*). The simultaneous presence of mechanical stability and self-healing behaviour is crucial in developing such hydrogels.

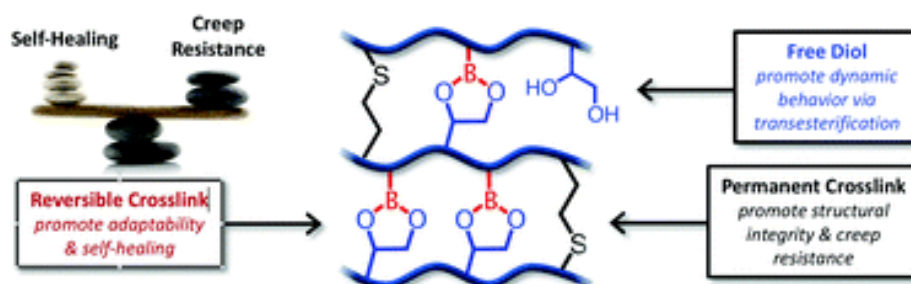


Figure 9. Reversible and permanent crosslinks between polymer chains.

To prepare self-healing hydrogels, boronic acid and its derivatives are widely used. The boronate ester bond can form through the reaction between boronic acid and a diol. It is a reversible bond, sensitive to changes in pH and temperature. Catechol groups are often utilized in the design and synthesis of self-healing hydrogels characterized by boronate ester bonds chemistry. In *Figure 10*, an example of a boronate ester bond formation is represented.

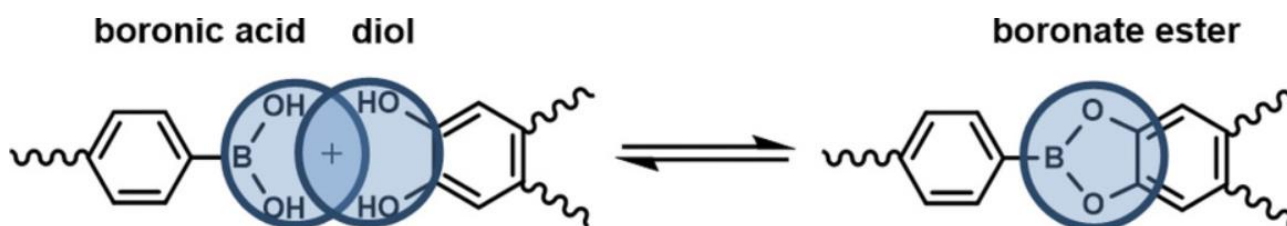


Figure 10. Example of reaction between boronic acid and a diol with consequent boronate ester bond formation.

Cash et al. synthesized a self-healing hydrogel capable of repairing its structure via the establishment of dynamic covalent bonds exploiting the boronate ester bond reversibility. Self-healing ability was investigated studying the bulk behaviour of polymeric networks characterized by the incorporation of boronic ester diene molecules, prepared with the reaction between 4-Vinylphenylboronic acid (VPBA) and 3-allyloxy-1,2-propanediol in a dry organic media. The reaction leading to the cross-linked network is a thiol-ene reaction, involving two thiols in different concentrations, which were pentaerythritol tetrakis(3-mercaptopropionate) (PTMP) and 3,6-dioxa-1,8-octanedithiol (DODT). The resulting hydrogels were able to self-heal at room temperature. The samples were cut, healed, and dried for several cycles. Two ways of self-healing were analysed, the first one consisted in adding minor amounts of water on the cut surfaces of the samples in order to achieve free boronic acid groups and diols, leading to the healing via boronate ester bond formation. The second way is the same as the first procedure without adding water on the surfaces. The results showed that the addition of water made the hydrogel self-heal faster and more efficiently. To prove that the self-healing behaviour was relatable to the boronic ester bonds established, control samples were tested. In the control sample, the boronic ester diene was substituted with divinylbenzene. Here, no healing was observed after four days, demonstrating the boronic ester bond reversible nature importance in the self-healing process. To study the mechanical properties, tensile tests were conducted and demonstrated that the material composed of 75:25 DODT:PTMP was able to self-heal for three cycles, recovering almost fully the initial tensile strength and elongation at break [27].

Boronate ester bonds can be achieved exploiting other boronic-based molecules, such as borax. He et al. synthesized a self-healing hydrogel via thiol-ene reaction between PEGDA and DTT. Here, the borax in its anionic configuration, induced the formation of transient boronate ester bonds between its hydroxyl groups and the DTT's exposed hydroxyl groups. Due to the borax diol complexation, a network with inter-chain linkages is formed. Thus, the resulting hydrogel demonstrated the ability to self-heal thanks to the dynamic nature of these boronate ester bonds. Samples were cut and then reassembled. Healing occurred within 30 minutes, and the gels could withstand their weight. Furthermore, the hydrogel demonstrated the ability of dissociating and reassociating according to the pH or temperature. In particular, at pH=3 the hydrogel network was dissociated; reassociation occurred when pH was set to 9. The same result was obtained when temperature was adjusted to 80°C, leading to the cross-links degeneration. Regeneration took place when the material was cooled down to 18°C. This result was achieved even after three cycles of self-healing. The mechanical properties are comparable to the ones characterizing permanently cross-linked PEG gels. The storage modulus reached up to 10^4 Pa. This indicates the capability of this hydrogel to provide the mechanical support needed for hydrogel scaffolds [28].

The possibility to transfer the dynamic properties to materials via integration of small molecule kinetics such as borax was demonstrated in Cromwell et al. work. They described how, varying the rates of boronic ester transesterification, the malleability and self-healing properties of the hydrogel can be tuned. They used telechelic diboronic ester molecules and 1,2-diol-containing polycyclooctene polymer to obtain dynamic cross-links. Studying the effect on self-healing of two different diboronic ester molecules as cross-linkers, only one demonstrated to be able to make the hydrogel recover its properties. This result indicated that the variability in healing efficiencies and the bulk gel properties are directly connected to the effect of small cross-linking molecules kinetics. Self-healing tests were performed also on control samples to assess that the self-healing was effectively related to the boronic ester bonds chemistry. Mechanical properties such as Young's modulus and ultimate tensile strength were recovered almost fully after three cycles of self-healing. Hydrolytic stability of boronate ester linkages was also tested immersing the samples in water overnight. Mechanical properties and mass showed no changes, suggesting that the hydrophobic environment of the polymer system shielded the boronic ester linkages from hydrolysis [29].

2.2 Non-covalent interactions

A non-covalent interaction, unlike covalent bonds, involves dispersive Debye-type interactions in a molecule or between molecules, which can be permanent (ions interaction), induced (ions+ induced dipole) or secondary (e.g. H-bonds and π - π interactions). Secondary forces play a crucial role in maintaining the 3D structure of large molecules, such as proteins or enzymes. Hydrogels can be prepared implementing non-covalent interactions in the polymeric network such as electrostatic interactions, hydrophobic interactions, host-guest interactions and hydrogen bonds. In the experimental part of this thesis, part of the self-healing ability of the synthesized hydrogel relies on hydrogen bonding; for this reason, more examples about this type of interaction will be reported. Non-covalent interactions are characterized by low intermolecular forces, so they are weaker compared to covalent interactions; thus, they are less stable and more sensitive to environmental changes and in certain pH or temperature conditions. Nevertheless, hydrogels with good mechanical stability can be prepared exploiting these interactions, which can enhance self-healing performances.

2.2.1 Electrostatic interaction

This class of non-covalent interactions, also called ionic interactions, occur between charged species. The force of the interaction can be repulsive if the species are similarly charged ions, attractive if it involves oppositely charged ions. Many synthetic materials and biological structures functions are based on this type of interaction, which is based on Coulomb's law. In self-healing hydrogel preparation, implementing electrostatic interactions between species in the polymeric network can facilitate the material's ability to recover after damage due to the re-establishment of these interactions across the material's interfaces. Self-healing hydrogels can be prepared through electrostatic interactions using polyelectrolytes, polyampholytes, charged polymers and zwitterionic fusions.

The strength of the electrostatic interactions can be tuned controlling the concentrations of the polyelectrolytes in the network. The opposite polyelectrolytes form polyion complexes (PIC), which are characterized by the presence of stronger and weaker cross-links. Usually, the weaker electrostatic interactions are the ones that can break and reform in response to damage, while the stronger interactions give the hydrogel an elastic behaviour and overall mechanical stability. PIC approach is widespread and easily applicable to different types of polyelectrolytes, and it leads to

the possibility of producing hydrogels with versatile mechanical and chemical properties. Unfortunately, the reaction producing the PIC is very fast. This can lead to non-homogeneous networks if the mixing is made with bulk solutions. To avoid this problem, Luo et al. prepared a PIC hydrogel mixing a cationic monomer, which was polymerized in advance, with a solution of an anionic monomer, which was polymerized after well dispersion. Polymers were prepared in a 1:1 charge ratio. After, they immersed the sample in water (dialysis) to remove counterions and obtained a tough PIC hydrogel at equilibrium. After the dialysis, the material is much tougher than before, and accordingly, the mechanical performances of the hydrogel increased drastically (elastic modulus of 5.4 MPa). The authors attribute this change to the high number of interchain complexes that are formed during the dialysis in water. Self-healing was performed with the aid of a NaCl solution. Mechanical tests after self-healing showed that the PIC hydrogel performed good recovery. Different PIC hydrogels were prepared and tested, showing different results regarding their mechanical features. Therefore, by exploiting electrostatic interactions, it is possible to prepare self-healing hydrogels with versatility. In fact, through the choice of the polyelectrolytes and their concentrations, mechanical properties can be tuned as well [30].

2.2.2 Hydrophobic interaction

Hydrophobic interactions are related to nonpolar molecules which tend to aggregate in aqueous environments. Reversible physical cross-links can be created exploiting this chemistry, enabling self-healing. When ruptures or damages to the hydrogel occur, the hydrophobic segments can re-associate in water healing the network structure. To achieve good results in these terms, some crucial parameters must be considered. It is important to balance the quantities of hydrophobic and hydrophilic units, the stability of the cross-links and the presence of surfactants, which are responsible for the reversible behaviour of hydrophobic cross-links. Additionally, the presence of electrolytes is also important [31].

Often, surfactant micelles are employed as cross-linking points to build the polymeric network structure via micellar polymerization of hydrophobic and hydrophilic monomers, one of the most used techniques. Also, this type of hydrogel can be prepared without using a surfactant. Owusu-Nkwantabisah prepared a self-healing hydrogel making an aqueous polymer solution (with a certain polymer concentration) evaporate; in this way, the gel will form via hydrophobic associations [32].

For example, Okay et al. managed to synthesize a self-healing hydrogel making copolymerize hydrophobic monomers of stearyl methacrylate (C18) with hydrophilic monomers of acrylamide

(AAM). Surfactant sodium dodecyl sulfate (SDS) and NaCl were added to the solution as well. The resulting mechanical properties and self-healing behaviour were great, achieving elongation ratios up to 3600% and 100% self-healing recovery. The hydrogel healed within seconds at room temperature. The influence of SDS on the mechanical performances and self-healing efficiency was crucial [33]. Therefore, it is possible to prepare self-healing hydrogels with excellent properties via hydrophobic interactions, exploiting the properties of the micelles to create physically cross-linked architectures.

2.2.3 Host-guest interaction

Self-healing hydrogels can be prepared by incorporating host molecules and their corresponding guests in the polymeric structure. It is a versatile mechanism since a wide variety of molecules can be used for this intent. This interaction involves the reversible binding of a host with its guest molecule; typically, the host molecule is a big cyclic molecule and has a binding site, that could be a cavity, where the guest can accommodate via non-covalent interactions such as π - π stacking, electrostatic interactions, hydrophobic interactions, van der Waals forces, and hydrogen bonding. Several self-healing hydrogels have been prepared exploiting as host molecules cyclodextrins (CDs), which are oligosaccharides with an α -1,4-glucose linked units, characterized by a hydrophobic internal cavity. These types of hosts can encapsulate various guest molecules. For example, Masaki et al. designed a self-healable polymeric material based on supramolecular and polymeric chemistry using multipoint recognition between cyclodextrin and guest hydrophobic molecules present on the polymer side chain. In particular, they used water-soluble polymer backbones modified with β -cyclodextrin (β CD) and adamantane (Ad) at the side chain. The gel demonstrated the ability to self-heal due to the reversible nature of the host-guest interaction implemented in the network. The content of host-guest moieties and their role in influencing the mechanical behaviour of the gel has been studied, finding an optimal concentration of these moieties. Low density polymer network brings disadvantages to self-repair abilities because of the poor number of interactions. On the other hand, if the polymer network is too dense, the mobility of the host-guest molecules may be inhibited, resulting in a negative effect toward the gel self-healing. Mechanical tests showed that the resulting host-guest gel has high toughness and elastic deformation behaviour. Additionally, self-healing ability was confirmed and possible either in wet or dry conditions [34].

2.2.4 Hydrogen bond

A hydrogen bond involves a hydrogen atom and a highly electronegative atom, which can be oxygen, nitrogen, or fluorine. The displacement of this partial positive charge and negative charge establishes a physical electrostatic interaction between moieties located on different polymer chains. This type of attractive interaction is weaker compared to covalent or ionic bonding, but it can be present all over the network, contributing to determine the hydrogel bulk properties, possibly enhancing the overall strength of the 3D network. In fact, hydrogen bonding can be integrated in the polymeric network with other types of bonds to enhance also the self-healing ability of the gel. In order to obtain a large number of these bonds, polymers with many hydroxyl groups are useful for this purpose. In this frame, Zhang et al. have developed a self-healing hydrogel via freezing/thawing method made of poly (vinyl alcohol) (PVA), a polymer which contains lots of hydroxyl groups. They investigated the self-healing efficiency and found that it was directly connected to the number of PVA chains free hydroxyl groups on the cut surfaces and PVA chains mobility. The self-healing was performed at room temperature and without the need of other stimuli or healing agents. Hydrogel production is easy and low cost. Also, this hydrogel is biocompatible and nontoxic. Regarding the mechanical properties of this PVA hydrogel, tensile tests were performed and showed that the recovery of mechanical features such as elongation at break and tensile strength increased when the healing time was increased. For example, after 48h of healing, the tensile strength was 200 kPa, which was the 72% of the pristine sample's tensile strength. The same test was performed also on the sample healed for 10 minutes, where the tensile strength was 50 kPa (20% recovery). Here, they demonstrated the importance of the time needed by the PVA chains to rearrange and heal via the establishment of hydrogen bonding [35].

Exploiting the same freezing/thawing method, Li et al. prepared a PVA self-healing hydrogel incorporating melamine, a molecule capable of forming multiple H-bonds with PVA. Results showed that tensile strength and elongation at break increased compared to PVA hydrogels, respectively by 420% and 160%. Furthermore, ultrasound triggered shape recovery of the hydrogel [36].

Another PVA-based hydrogel was developed by Le et al. which showed complete self-healing behaviour. The synthesized hydrogel's polymeric network was constituted by PVA-sodium alginate-borax (PVA-SA-borax). Sodium alginate was added to improve the stretchability of the PVA-borax crosslinked network. Self-healing occurred completely in 3 h. Moreover, the hydrogel showed good barrier properties to some chemicals like sodium cyanide [37].

Lijun et al. developed a sensing material which is a PVA hydrogel based on borate bonds and hydrogen bonds containing also graphene oxide (GO). They constructed a physical-chemical double cross-linked PVA-borax-GO able to self-repair at room temperature that showed great mechanical properties. The presence of the borax in the network provided self-healing via dynamic covalent bonds which form with PVA and GO. The hydrogel has an elastic behaviour, it is stable and conductive, due to these properties it is interesting in the sensing materials field [38].

3. 3D Printing

3.1 3D Printing overview

3D printing, also known as additive manufacturing, comprehends technologies that enable the creation of personalized three-dimensional objects starting from STL models. 3D printing has gained interest due to its numerous applications in research and industries such as healthcare and aerospace. Various techniques are part of the 3D printing field, and each has its own strengths and limitations. Each technique offers its own benefits in terms of precision and material variety; thus, 3D fabrication is considered to be a versatile and rapidly advancing field. Generally, 3D printing processes differ from the traditional subtractive manufacturing methods due to the fact that the objects geometries are obtained adding material layer-by-layer rather than removing it. Given this, 3D printing is considered to be more sustainable than traditional processes. These bottom-up technologies build the objects gradually, using the geometrical information contained in STL files, which are created via computer aided design (CAD) software. STL files store coordinate information of a 3D object that describe its geometric shape without representing colour or textures. To print layer by layer, the 3D object is sliced into X-Y horizontal sections. These thin sections contain the geometrical information of every layer, which will be printed gradually starting from the one at the bottom. Following these steps, the object will be printed along its Z axis [39].

Adjusting printing parameters and selecting the technique that fits better for the purpose, several shapes and geometries can be obtained. Moreover, given the wide range of materials that can be used to print 3D objects, it is possible to achieve the desired mechanical and chemical properties of the final objects. 3D printing techniques can be divided in three categories according to the printing mechanism technology features [40].

The first category comprehends a set of extrusion-based methods for which liquid thermoplastic polymers are extruded on a plate on which they solidify. This technology works by melting polymer

filaments extruding it through a heated nozzle, depositing the material layer by layer to build up the 3D object. The solidification usually occurs in a very short time. The most widespread of these techniques is Fused Deposition Modelling (FDM), in which are commonly used material as polylactic acid (PLA), polyethylene terephthalate glycol (PETG) and other thermoplastics [41].

Powder-based methods utilize powdered materials to create objects by fusing or binding the powder in precise patterns. Generally, the process starts spreading a thin layer of powder on the build platform. Then a laser scans the layer and based on the technique, it makes the powder solidify or melt. For example, in Selective Laser Sintering (SLS) the first layer will be scanned by a laser which sinters the powder locally according to the desired geometry. After this, the platform moves down, and a new layer of powder is spread. After repeating these steps, the final object is obtained. The excess powder can be removed and reused. Some other powder-based techniques are Electron Beam Melting (EBM), Multi Jet Fusion (MJF) and Binder Jetting [42].

The third category includes photopolymerization methods. Here, liquid polymer resins are cured into solid structures via irradiation of UV light. The polymerization occurs relatively fast and does not require high temperatures. In a photocurable resin, the components must include monomers and photoinitiators at least. Other elements can be added, such as fillers, dyes and radical scavengers [43].

Techniques as Stereolithography (SLA), Digital Light Processing (DLP) and Continuous Liquid Interface Production (CLIP) exploit photocurable resins and 3D objects with high resolution can be produced. The cited techniques are included in Vat Photopolymerization (VPP) technology. Through VPP, photo curable liquid resins are poured in a tank, known as vat, in which photopolymerization occurs via irradiation provided by a light source. This technology gained significant attention due to its high accuracy, high speed, and wide range of applications in functional devices development [15] [44].

Since this thesis work consisted in developing a photocurable resin for VPP 3D printing of a biocompatible self-healing hydrogel via DLP, photopolymerization process and VPP techniques will be explained in detail in the next paragraphs, with a focus on DLP.

3.2 Photopolymerization process

Photopolymerization is a process in which liquid reactive solutions undergo through a chemical reaction driven by the light, that ultimately leads to phase change and solidification. Typically, UV light is used to activate this reaction since ultraviolet light brings more energy than other types of radiation, being in any case relatively safe if properly confined. The above-mentioned formulations are basically a mixture of monomers, oligomers and photoinitiators. As mentioned, in those resins can be included also additives like fillers, dyes and radical scavengers. In paragraph 3.2.2 a more detailed explanation about these components is reported.

The photopolymerization reaction starts with the activation of the photoinitiator. Absorbing light, the photoinitiator produces reactive species like free radicals or cations which reacts with specific functional groups on the monomers (e.g. C=C double bonds), starting the polymerization process. The photoinitiator activation is achieved only if its absorption spectrum and the light emission spectrum are overlapped [45].

Depending on the nature of the reactive species that lead to the formation of the polymeric network, two main mechanisms can be identified: radical mechanism, which involves radicals, and ionic mechanism, which involves ions (cations or anions).

In the next paragraph, these polymerization mechanisms will be explained. Following, thiol-ene reaction will be described too since it occurs during the printing process of the developed self-healing hydrogel. In particular, when the synthesized resin is exposed to UV light, PEGDA undergo radical chain-growth polymerization as DTT reacts with PEGDA and HEMA via thiol-ene step-growth polymerization. Both reactions are polyadditions that occur due to the continuous reaction of propagating species with unreacted monomers.

3.2.1 Photopolymerization mechanisms

In general, two mechanisms can be followed by a photocurable system: free-radical mechanism and ionic mechanism.

Free-radical mechanism: photo curable materials that follow this mechanism to polymerize go through chain-growth polymerization. This process is characterized by three phases, which are initiation, chain propagation, and termination (side reactions can occur). During initiation reactive species are formed through the action of a photoinitiator. In chain propagation phase, these reactive

species, which are radicals, react with monomers. These monomers are gradually added to the chain reacting with the active center (atom with an unpaired electron) on the growing polymer molecule, leading to the formation of the final polymer chain. The efficiency of the process may be limited by oxygen inhibition: the atmospheric oxygen can extinguish the initiators by binding with free radicals [46].

Termination occurs when the active center disappears. Usually, in radical reactions this happens due to the reaction between two radical chains, following a process called combination. The chain termination can also occur via another mechanism, called disproportionation, which typically involves the reaction between impurities and radicals. Consequently, the polymerization terminates. Free-radical polymerization is mostly used in biomedical applications due to its high rate of polymerization [47].

Ionic mechanism: in this process, monomer functional groups that undergo cross-linking are activated through the action of an ionic photoinitiator. This mechanism involves either the generation of cationic or anionic species to initiate and propagate the polymerization reaction. Usually, ionic photoinitiators have cationic nature. Once excited, dissociation of a counter anion takes place, generating a reactive carbocation on a radical. The carbocation adds to another monomer, propagating the chain reaction. Termination occurs following the disproportionation process when the polymer chains react with impurities or other inhibitor molecules.

In *Figure 11*, examples of these two mechanisms are reported.

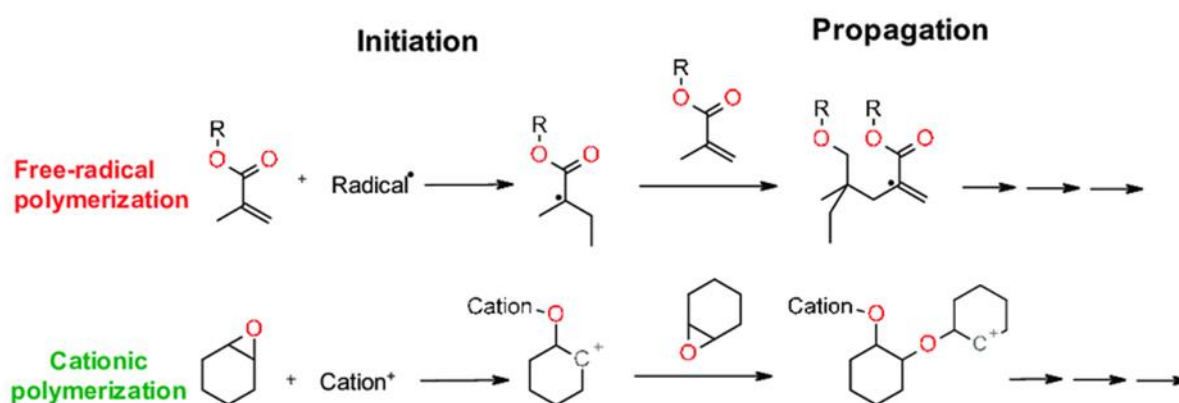


Figure 11. Examples of free-radical and cationic polymerization mechanisms.

Thiol-ene reaction: this is a type of click chemistry reaction between a thiol (R-SH) and an alkene (C=C) to form a thioether (R-S-R') as shown in *Figure 12*. This reaction is highly valued and considered in materials science for its selectivity, high conversion rate and mild reaction conditions. The reaction

typically goes to completion quickly and is compatible with a various range of functional groups, making it versatile. Also, this reaction can take place in aqueous solutions due to the non-interference of water; thus, it can be useful in hydrogel synthesis.

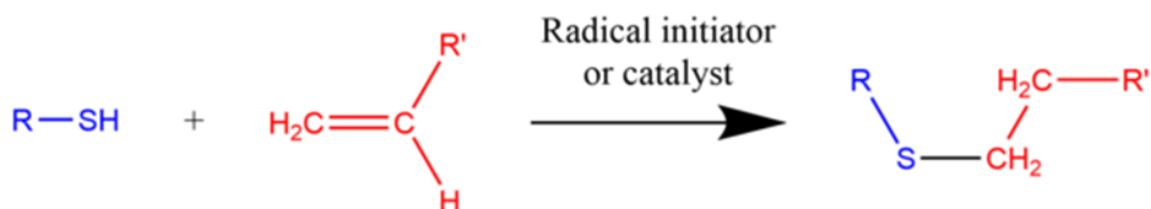


Figure 12. Example of a thiol-ene reaction between a thiol and an alkene.

Thiol-ene reactions can proceed following two main mechanisms: thiol-Michael type reactions and free-radical additions.

Usually, thiol-Michael type reactions are catalyzed by a base which abstracts a proton from a thiol, forming a thiolate anion. The thiolate anion, acting as a nucleophile, attacks the electrophilic- β carbon of an alkene to form a carbon-centered anion intermediate, which abstracts a proton from the conjugated acid to generate the final product. The reaction keeps going until the last reactive group is consumed and is usually side products-free [48]. In *Figure 13A* an example of this mechanism is reported.

In thiol-ene free-radical additions, to initiate the reaction, radical generation is needed. This can be achieved through a photochemical, thermal, or oxidation-reduction process. The reaction proceeds as the traditional free-radical polymerization and it involves three steps: initiation, propagation and termination. Photo- or thermoinitiation occurs with the decomposition of thiols into thiyl radicals (RS^\cdot) through hydrogen abstraction. In the propagation phase thiyl radicals attack the alkenes double bonds, forming thiol-ene addition products as shown in *Figure 13B*. The unpaired electron from the carbon centered radical is transferred to another thiol group and the cycle restarts. This propagation is characterized by high yield, and it is less sensitive to oxygen inhibition compared to traditional free-radical chain polymerization. Termination occurs via radical recombination rather than disproportionation [48] [49].

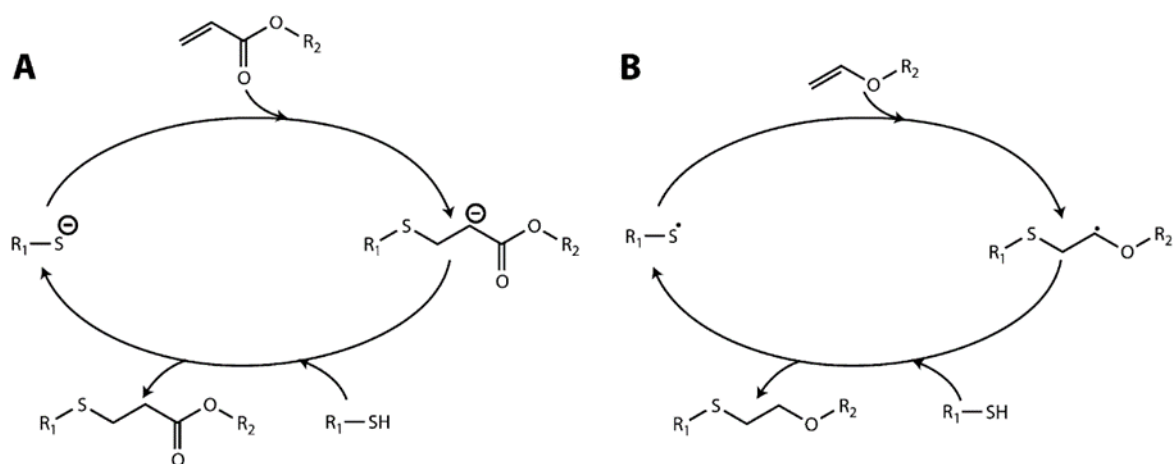


Figure 13. Thiol-ene reaction mechanisms via Michael type reaction (A) and free-radical addition (B).

Another example highlighting the thiol-ene step-growth polymerization process is reported in Figure 14.

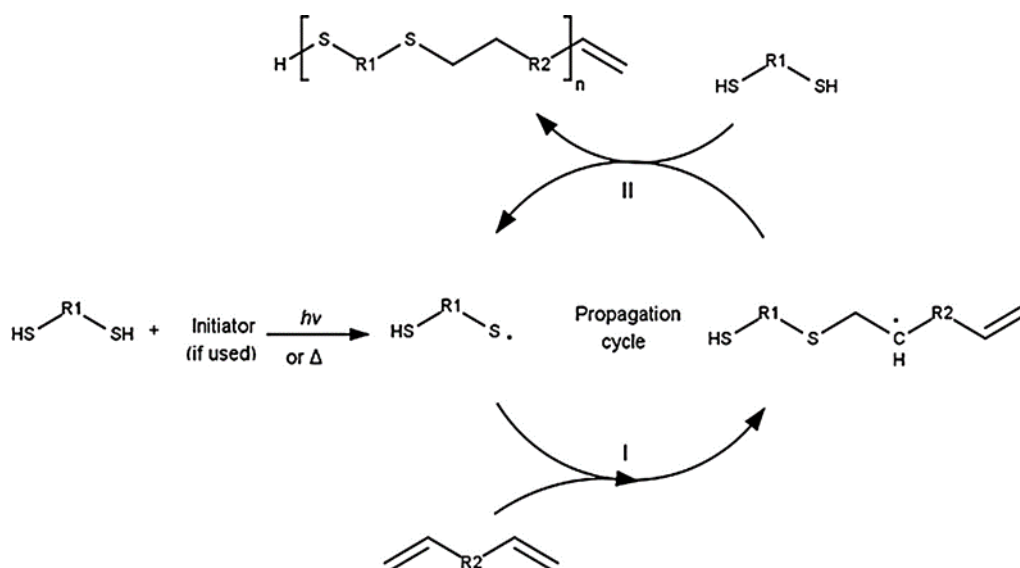


Figure 14. Thiol-ene step-growth polymerization between diacrylate and dithiol species.

The radical thiol-ene reaction is considered a versatile methodology for the preparation of cross-linked networks. As mentioned, it can proceed in the presence of air or aqueous environment, and it is metal catalyst-free [50]. For these reasons, it is considered a powerful technique to obtain hydrogels for biomedical applications.

For instance, Wang et al. produced a biocompatible and biodegradable hydrogel using 5-ethyl-5-(hydroxymethyl)-b,b-dimethyl-1,3-dioxane-2-ethanol diallyl (EHDA), a diallyl cyclic acetal monomer, and pentaerythritol tetrakis (3-mercaptopropionate) (PETMP), a multi-thiol. These two molecules copolymerized and formed the hydrogel network. Cytotoxicity was evaluated *in vitro* on fibroblast

cells. Fluorescence microscopy revealed that the cells attached to the structure were capable of growing. Also, the cell nucleus morphology was normal. This suggested that the cells could function biologically on this material. Lastly, non-toxicity on fibroblast and overall biocompatibility were confirmed [51].

In another work, a PEG-based hydrogel containing β -cyclodextrin (β -CD) was prepared via radical-induced thiol-ene click chemistry. Linear bifunctional PEG chains contained two allyl groups while the crosslinkers were heptavalent thiol-functionalized β -CDs. Physical features such as water uptake capacity and rheological properties were evaluated using different PEG chain lengths and varying the crosslinker concentration. Also, the controlled release of a drug named puerarin was analysed and found to be dependent on the composition of the hydrogel and showed that it could be used for drug delivery purposes. Arslan and his colleagues were also able to fabricate hydrogel microstructures on solid substrates [50].

In another study, the development of a norborene functionalized alginate hydrogel is reported. This system functioned as a cell-laden bio-ink for extrusion-based bioprinting, in which the rapid UV-induced thiol-ene crosslinking was exploited to achieve 3D bioprinted constructs. It was demonstrated that the bioink was modulable in terms of mechanical and swelling properties by varying the concentrations of dithiol PEG cross-linkers. Moreover, the ability to tailor the gel properties and biofunctionality (e.g. RGD attachment) allowed the authors to design multizonal and multicellular constructs for TE applications [52].

3.2.2 Photocurable resin components

Commonly, a liquid photocurable resin is composed of at least one photoinitiator and monomers/oligomers. In addition, ingredients such as dyes, fillers and radical scavengers can be added to improve printability and impart specific characteristics to the material. The role of the components will be described in detail in the next sections.

3.2.2.1 Monomers and oligomers

Monomers, or oligomers, are photoreactive precursors which frequently undergo free-radical polymerization reactions and are typically characterized by acrylate functional groups. Monomers are small molecules with low molecular weight and one or more reactive groups. Oligomers are chains of monomers (typically 2-20 units) which often have at least two reactive groups [53].

They represent the building blocks of the polymeric chains that will constitute the cross-linked network. Final mechanical and physical properties like toughness and flexibility depend mostly on the precursor backbone, while the polymerization kinetics is controlled by the reactive groups. Based on the application, monomers or oligomers for VPP are selected according to their functionalities. Systems based on various functional groups such as thio-ene, vinyl-eter, vinyl, polyester, (meth)acrylates, (meth)acrylamides can be prepared. Other features which need to be considered in order to regulate mechanical and chemical properties of the final product are viscosity, shrinkage, toxicity, costs, hydrophobicity/hydrophilicity, and functionality (mono-, di- or poly-) [54].

For 3D printing, it is preferable to have resins characterized by high polymerization rate, low shrinkage rate, low viscosity, high photo reactivity. Acrylic-based resins offer partial but still good compatibility with these features, reason why they are commonly used in 3D printing and are suited for various commercially available 3D printers. In particular, acrylic resins have the advantage to undergo photopolymerization via radical chain-growth mechanism, which is fast and highly reactive. On the other hand, these resins tend to shrink while printed, and this can lead to dimensional inaccuracies in the final part. However, the shrinkage rate can be adjusted to avoid, at least partially, these kinds of problems. For example, the use of methacrylate monomers can reduce this problem, but it lowers the curing rate. Also, oligomers with high molecular weight and less reactive groups can be exploited to make the resin shrink less. Still, this leads to restricted mobility and resins with high viscosity, so heat can be required. Moreover, during the printing process in a vat open system, the resin can be exposed to oxygen which can react with free radicals interrupting the polymerization. To mitigate such issue, additives can be used to reduce oxygen inhibition. Commonly used acrylic resins in VPP 3D printing are PEGDA, 2-Hydroxyethylacrylate (HEA) and bisphenol A ethoxylate dimethylacrylate (BEMA) [54].

Other systems, such as thiol-ene and epoxy systems can offer reduced shrinkage and higher conversion compared with acrylates. Thiol-ene networks are formed under ambient conditions via radical step-growth polymerization, the process is characterized by high conversion and reaction rates. Other advantages are the lower sensitivity to oxygen inhibition and less brittle materials as result. Also, if allowed by the exploited chemistry, hydrogen bonding between the network chains can be adjusted leading to a higher rigidity [55].

However, these systems typically have poor mechanical properties compared to the acrylate-based systems. To take advantage of the optimal features that characterize acrylate and thiol-ene -based

systems, a mixed resin can be prepared combining the rapid curing and mechanical strength of acrylates with the flexibility and reduced shrinkage of thiol-ene chemistries.

3.2.2.2 Photoinitiators

In a photocurable resin, a photoinitiator (PI), or photoinitiator system, is the element responsible for converting photons energy into reactive species after light irradiation. PIs can be either radical or cationic, depending on the nature of the reactive species generated. These species react with monomers or oligomers, starting the polymerization process. Photoinitiating systems determine the mechanism of the reaction, affect its curing speed, and mechanical and rheological properties of the final object. To initiate the process and gain good efficiency, it is crucial that the emission spectrum of the 3D printer overlaps with the PI absorption spectrum. Different PIs are activated at different light wavelengths. The wavelengths can be within UV (190-400 nm), visible (400-700 nm), or infrared (IR) range (700-1000 nm). The majority of the PIs react within the UV and visible light ranges, and these are compatible with all VPP techniques. For example, in common DLP, light is emitted at 385/405 nm. For these reasons, PI, precursors and the wavelength range of the light source must be chosen accordingly [14] [54].

3.2.2.3 Dyes

In photocurable resins, the presence of the dyes affects how light penetrates and cures the resin. For this reason, dyes enable control over light absorption. In fact, they are used in 3D printing to achieve good printing resolution controlling the polymerization. Also, they can be used to customize with colours parts of the object for aesthetic reasons. Common dyes absorb light in UV and visible range. To play their role, it is necessary that the dyes absorption spectrum matches with the emission spectrum of the printer. For example, methyl red is used in acrylate-based resins to achieve high printing resolution.

3.2.2.4 Fillers

In order to modify the mechanical, electrical, physical properties of the printed material, fillers can be added. Fillers are divided into organic (natural polymers) and inorganic types (metallic or ceramic powders). They must be chosen taking into account that the resin must remain stable during the printing process. They can reduce the shrinkage and introduce controlled anisotropy, enabling spatial-controlled specific properties in the material. Also, through fillers, both warping effect and

heat expansion can be reduced. Carbon materials, ceramic and metal powders, glassy and fibrous materials as cellulose are examples of materials that fall into this category.

3.2.2.5 Radical scavengers

Radical scavengers (RS) are chemical agents that can remove undesired reaction products. Due to their antioxidant nature, they can act as radical inhibitors, de-activating free radicals in order to control the polymerization diffusion if needed. In this work, the developed resin contains a grape seed extract (a type of tannin), which is used as radical scavenger to regulate the diffusion of the polymerization during the printing process. Some polyphenol compounds have been reported to have good free-radical scavenging ability. In particular, He et al. found that by properly setting the concentration of tannic acid (TA) in the resin, it exhibited excellent anti-polymerization effect [56].

4. Vat Photopolymerization techniques

Vat 3D photopolymerization (VPP) based techniques enable 3D fabrication of complex material systems with controllable chemical and mechanical properties. 3D photopolymerization involves photoinitiators and monomers/oligomers in liquid state that can be cured after being exposed to light at different wavelengths (depending on the photoinitiator systems absorption characteristics). VPP strategy is based on light irradiation through a vat in which a photocurable resin is poured. The photopolymerization occurs on a building platform, in accordance with the illuminated area. The building platform moves vertically, so that only one layer of resin is exposed to light. High resolution (order of micrometers) can be achieved using versatile polymer chemistry, making this technology interesting for developing objects related to various fields, such as microfluidics, tissue engineering, drug delivery and others [14].

An advantage of these methods is the wide range of photocurable materials that can be used to produce object for various applications, such as organic-inorganic hybrid structures such as ferromagnetically responsive formulations [57].

Usually, no support structures are needed to print the construct. After the printing, some post-processing operations can be operated if needed. For example, solvents can be used to remove resin in excess. Additionally, in order to obtain a complete and more homogeneous polymerization, the printed object can be placed in a UV chamber for post-curing, resulting in better final mechanical properties. In the following paragraphs, the main VPP techniques (stereolithography (SLA), continuous liquid interface production (CLIP) and Digital Light Processing (DLP)) will be explained describing their characteristics and printing mechanisms.

4.1 SLA: mechanism and features

Typically, stereolithographic 3D printers use a liquid resin that solidifies when exposed to UV light from a punctual laser. Motors and mirrors control the laser to trace the cross-sections of objects in layers. The photocurable resin is poured into a tank and the laser beam irradiates it from above. The resin solidifies when scanned by the laser. The building platform is lowered into the resin so that its surface is a layer-thickness below the resin. After curing the first layer, the platform is lowered by one layer distance, and the process is repeated. The produced layers stack on top of one another until the final 3D object is obtained. The resolution that can be achieved with this technique can be up to 10 μm , good enough to print object with complex geometry and fine size. Resolution depends on the resin composition, laser speed and diameter of the laser spot [58] [59].

Depending on the model of the printer and its building platform dimensions, large sized objects can be printed through SLA (the largest the object, the lowest the printing rate). The main advantage of this technique is the resolution, which is better than that of DLP and CLIP [59].

A common setup of a SLA 3D printer is represented in *Figure 15*.

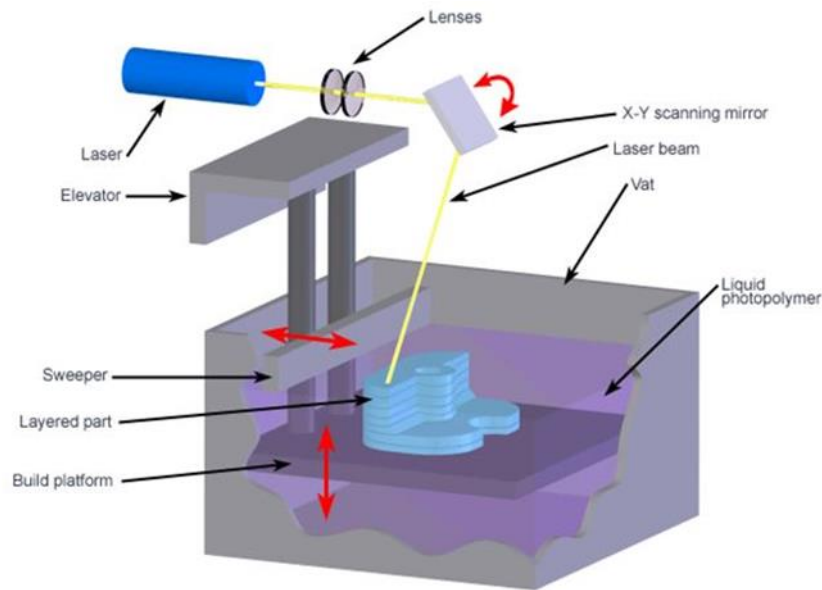


Figure 15. SLA 3D printer setup.

4.2 CLIP: mechanism and features

CLIP is an advanced 3D printing technology developed by Carbon3D. Compared to other techniques, it offers advantages in terms of printing speed (up to 100 times faster than DLP). Also, the layering can be infinitely precise [59].

Unlike traditional layer-by-layer 3D printing methods, with CLIP objects are created continuously, which results in faster printing times and smoother surfaces. The light source is positioned below the vat and the build platform is above, as in SLA and DLP. The peculiarity of this technology is the presence of an oxygen permeable window at the bottom of the resin bath. This window allows controlled amounts of oxygen to pass through, making it impossible for the resin to solidify in this layer. Above this window there's a zone called "dead zone", an uncured liquid layer, where free-radical polymerization is inhibited by oxygen. This inhibition is achieved in two ways: the photoinitiator is quenched by the oxygen, or via formation of a peroxide upon oxygen interaction with a propagating free radical [14].

From the bottom, the light source, usually a UV projector, irradiates continuously through the oxygen-permeable membrane into the resin vat. The resin solidifies in accordance with the illuminated area. As the resin is cured, the build platform continuously moves upward, pulling the object out of the vat. The most important advantage of this method is that the oxygen-permeable window ensures the continuity of curing, allowing for much faster printing times compared to other

techniques. A schematic representation of a CLIP 3D printer configuration with its elements is shown in *Figure 16*. However, to exploit the advantages of this technology, viscosity requirements must be satisfied. Rapid printing requires liquid photocurable resins that can rapidly move to the printing zone. To achieve this, the resin viscosity must be low enough to satisfy this fluidity requirement. If the resin viscosity is high, its bad fluidity may cause the lowering in the printing speed or even the failure of print. To sum up, the advantages that CLIP offers can be exploited only if the resin viscosity has a fluidity that permits to flow to the printing area in short times. In optimal conditions, printing times can be on the order of minutes, with resolution up to 100 μm [14].

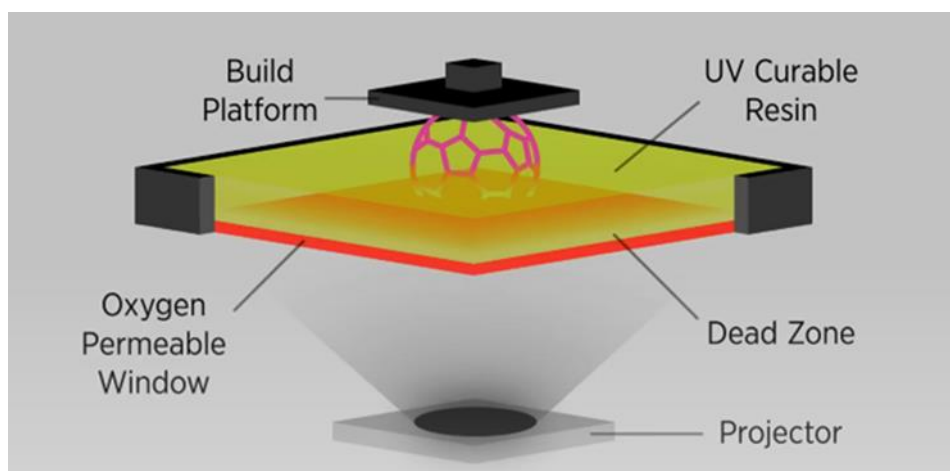


Figure 16. CLIP printer setup.

4.3 DLP: mechanism and features

Digital Light Processing 3D printing, as well as other VPP technologies, uses a vat in which a photocurable resin is poured. As SLA, the light source is positioned below the vat and the building platform is suspended above the resin bath. The light source is a built-in projector that sits under the vat. At each layer, The projector illuminates the entire area that correspond to the horizontal cross-sections of the 3D object, curing the entire layer at once. This is the main difference with SLA, in which curing occurs one spot at a time. In DLP, given that each layer of resin is illuminated and cured simultaneously, printing times are much shorter than those characterizing SLA. The key feature in DLP 3D printing is the digital micro-mirror device (DMD) inserted in the path of the laser. This technology determines the image formation with high precision. The DMD is composed of an array of thousands of micro-mirrors (each one corresponds to a single pixel) that can be powered on or off to let the UV light pass through or not, according to the desired illuminated area (*Figure 17*). The

DMD is oriented to project the entire layer image simultaneously by creating both illuminated and dark areas when illuminated by light [59].

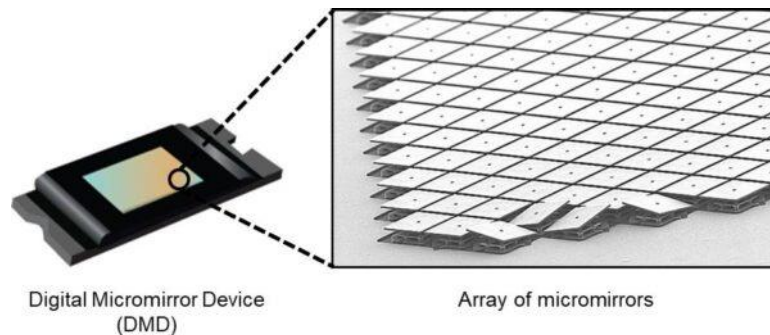


Figure 17. Digital Micro-mirror Device.

When the first layer curing occurs, the building platform moves upward a distance equal to the thickness of the layer. The process is repeated until the final 3D object is obtained.

In DLP, the typical light wavelengths used are 385 nm and 405 nm, and a resolution of 20 μm can be achieved [60].

The printing speed is one of the main advantages of DLP. High precision can be achieved limiting the size of the light projection; thus, through DLP smaller volumes may be printed [59].

In *Figure 18*, a schematic view of DLP apparatus is represented.

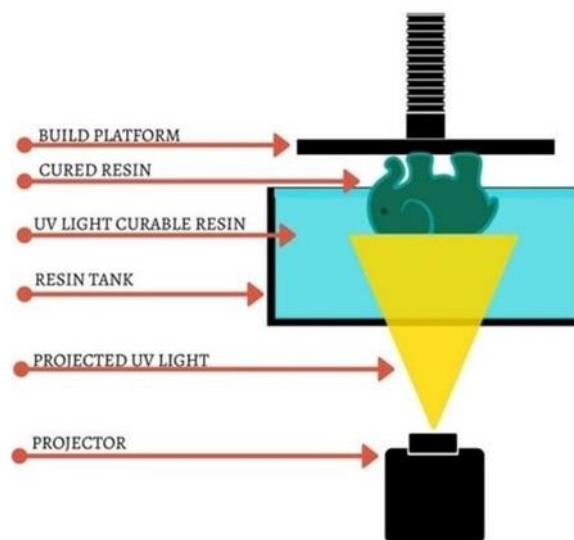


Figure 18. DLP printer setup.

Compared to SLA, the printing times in DLP are shorter due to the illumination of every layer at once, but the resolution is lower. Also, in DLP, the amount of resin needed is lower. Given the need in SLA

for the sample to be immersed in the resin, the amount of formulation needed is higher, and consequently the costs increase.

Regarding the DLP limitations, the main ones are related to the forces of attraction between the vat and the object being cured. The risk is that due to these forces, the object starts to solidify on the vat instead of the platform. To overcome this problem, coatings can be integrated to reduce the intensity of these forces [58].

Moreover, due to the optical technology implemented in DLP, the printed parts may tend to have a pixelated type of effect on surfaces of complex objects, while in SLA is possible to create smoother parts.

5. Materials and Methods

In this chapter, materials and methods used to prepare and characterize the photocurable resins for DLP 3D printing are reported.

5.1 Materials

The characterization analysis is conducted on acrylate-based resins. Formulations with different ratios of the following elements were characterized in order to find the optimal one in terms of mechanical properties, printability and ability to self-heal. Each characterized resin is composed of the following components:

PEGDA700: poly(ethylene glycol)diacrylate (PEGDA) gives structural integrity to the polymer matrix; it is a biocompatible photoreactive monomer known for his ability to rapidly cross-link when

exposed to light (typically UV) in presence of a photoinitiator. Resins with PEGDA as main polymer are characterized with good printability. This hydrophile molecule has two acrylate groups that lead to radical type polymerization.

HEMA: hydroxyethyl methacrylate (HEMA) is a monomer characterized by two functional groups: one acrylate and one hydroxyl group (OH). HEMA is added to introduce OH groups in the matrix, enhancing the stability of the network through the formation of hydrogen bonds between this pendant groups.

DTT: dithiothreitol (DTT) is used as a copolymer. Its linear molecular structure contains two thiol groups (SH) on the ends and the central portion exposes two hydroxyl groups. This polymer undergoes radical type polymerization with PEGDA and HEMA. The self-healing ability via the establishment of dynamic covalent bonds is based on the reversible reaction between the DTT's exposed OH groups and the functionalities of borax.

BORAX: borax (di-sodium tetraborate decahydrate) is a salt of boric acid. It is incorporated in the resin after being dissolved in PBS. In its ionic form, it presents an anion called tetrahydroxyborate which is a boron atom bonded to four hydroxyl groups. Boronate ester bonds can be established through the interaction between two tetrahydroxyborate's hydroxyl groups and the two DTT's exposed hydroxyl groups via transesterification reaction. This reaction can occur twice on both sides of the ion, involving two molecules of DTT present in two adjacent polymer chains, leading to the formation of inter-chain bridges capable to associate and disassociate reversibly. In *Figure 19*, a schematic representation is reported.

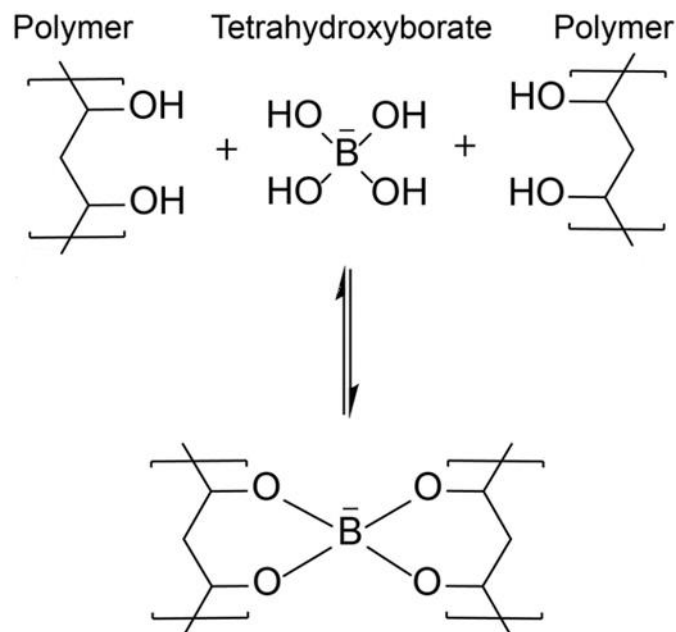


Figure 19. Example of a tetrahydroxyborate ion can bind on the sides of two polymeric chains.

LAP: lithium phenyl-2,4,6-trimethylbenzoylphosphinate (LAP) is the photoinitiator used in all formulations. It is a radical initiator that exhibits absorption in the UV range, so it is suitable to be integrated in the photocurable resin. In *Figure 20*, LAP emission spectrum is reported. The 3D printer emission wavelength is set at 385 nm. Looking at the LAP absorption spectrum it can be seen how it effectively absorbs at 385 nm [61].

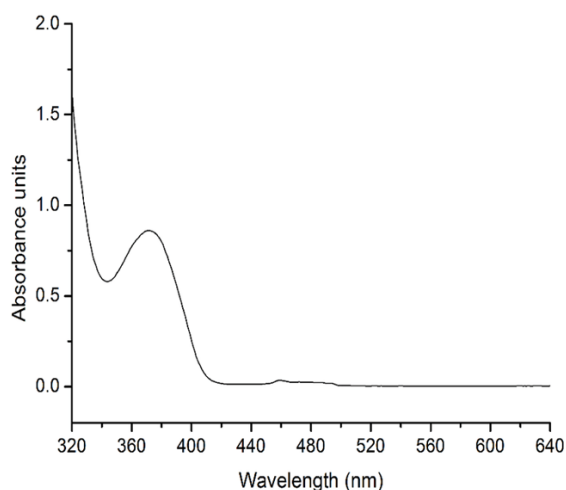


Figure 20. UV-Vis LAP absorption spectrum [61].

BAPO-OH: bis(mesityl)phosphinic acid (BAPO-OH) is a water-soluble photoinitiator synthesized in ETH laboratories (Zurich) by prof. Grützmacher. It is well soluble in water and hydrolytically stable for at least several weeks [62]. Its absorption spectrum is reported in *Figure 21*.

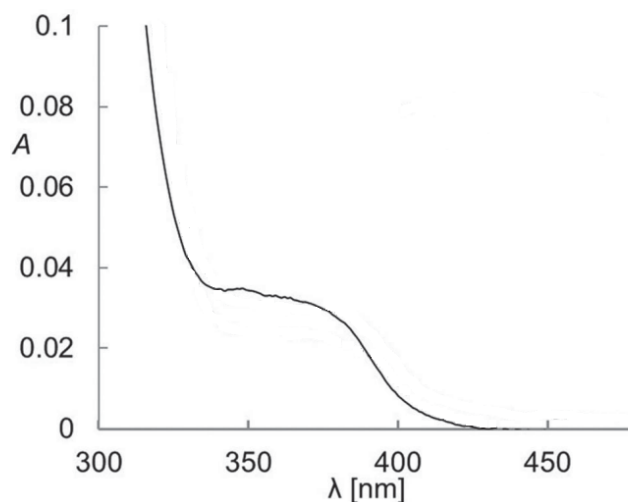


Figure 21. BAPO-OH absorption spectrum [62].

PBS: PBS (Dulbecco's Phosphate Buffered Saline) is a buffer solution (pH between 7-7.4) commonly used in biological research. It helps to maintain a constant pH. It is an isotonic water-based solution that contains different salts such as sodium chloride, potassium chloride and potassium dihydrogenphosphate.

Grapeseed extract: it is a powder derived by grape seeds and it is composed by tannins, which are polyphenolic compounds. In this work, it is used as a radical scavenger: polyphenols, in fact, are known for their antioxidant properties, and thus are able to interact with molecules generated in the irradiated areas that propagate out of those, stopping the polymerization. So, a radical scavenger allows us to limit undesired polymerization, increasing the printing resolution and allowing a more controlled polymerization process. This element is integrated in the resin mainly due to this property, but also because it is derived from a natural source.

Chemical structures of PEGDA, HEMA, DTT, tetrahydroxyborate ion, LAP and BAPO-OH are represented in *Figure 22*.

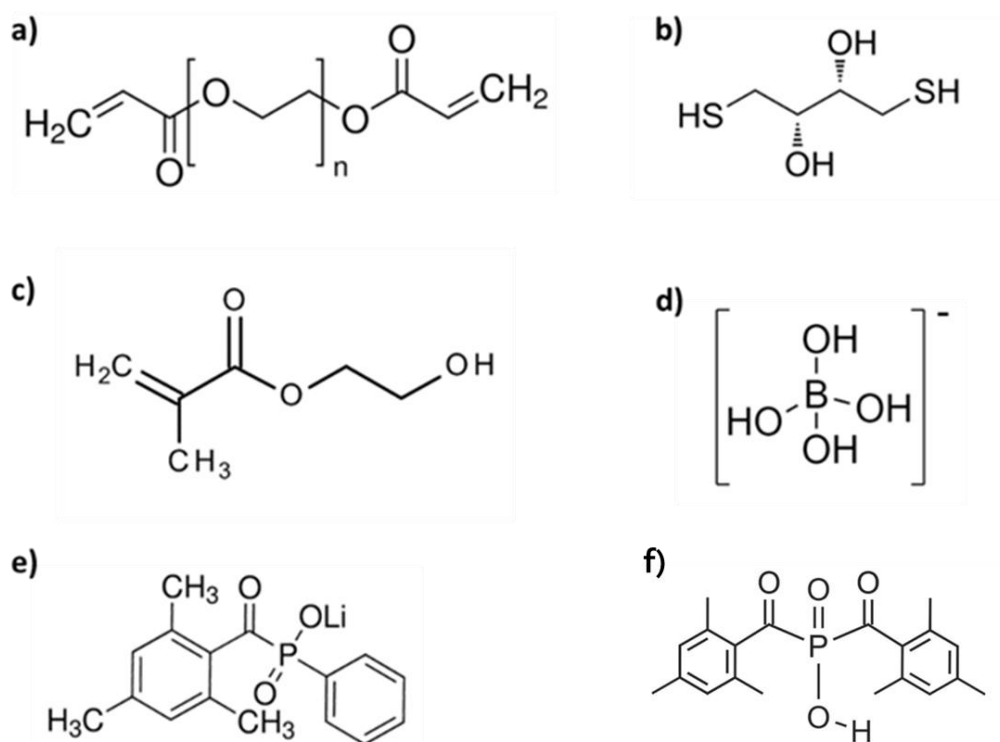


Figure 22. Chemical structures of (a) polyethylene glycol diacrylate (PEGDA), (b) dithiothreitol (DTT), (c) hydroxyethylmethacrylate (HEMA), (d) tetrahydroxyborate ion, (e) lithium phenyl-2,4,6-trimethylbenzoylphosphinate (LAP), (f) bis(mesityl)phosphinic acid (BAPO-OH).

PEGDA₇₀₀ (Mn = 700 g/mol), HEMA (99%, Mn = 130.14 g/mol), DTT (97%, Mn = 154.25 g/mol), LAP (>95%), borax (Mn = 381.23 g/mol) and PBS were purchased from Sigma-Aldrich (Merck Company, Darmstadt, Germany) and used as received.

BAPO-OH was purchased from ETH laboratories (Zurich, Switzerland) and used as received.

Grapeseed extract (Extratran Vinacciolo) was purchased from Oenoitalia Biotecnologie and used as received.

5.2 Formulations and preparation procedure

The tested formulations were produced varying DTT-borax ratio and DTT-acrylates ratio. All these different resins were produced with the following common ratios:

- 80% PBS
- 20% hydrogel
- HEMA : PEGDA = 1 : 2
- 1% LAP, calculated on acrylates weight
- 0,5% grapeseed extract, calculated on total weight (not considering LAP)

In *Table 1*, the two formulation sets are reported with their ratios. In B formulations, borax-DTT ratio is fixed at 1:3. In P formulations, acrylates-DTT ratio is fixed at 2:1. Therefore, B3 and P3 coincide.

NAME	PEGDA + HEMA	DTT
B1	1	2
B2	1	1
B3	2	1
B4	3	1
B5	4	1
NAME	BORAX	DTT
P1	1	1,5
P2	1	2
P3	1	3
P4	1	4
P5	1	5

Table 1. Classification of the produced and characterized resins.

The preparation procedure is common for all the formulations and consists of the following steps:

1. In a foil-covered vial (vial A), weigh the HEMA and calculate the corresponding amounts of the other components.
2. In a second foil-covered vial (vial B), add borax and PBS to prepare a 0.1M solution, then sonicate until dissolved.
3. In vial B, add DTT and sonicate until dissolved.
4. In vial A, add PEGDA, PBS, and LAP.
5. Place vial A in a dark Falcon tube to limit any possible interaction with light, then shake manually until LAP is dissolved.
6. Combine the contents of the two vials and gently shake manually.
7. Add the grape seed extract and dilute it using a magnetic stirrer.

5.3 DLP 3D printer and sample preparation

Nearly all the samples were prepared via DLP 3D printing. Some samples for qualitative self-healing tests were prepared with a Broad-band UV chamber from Asiga (light intensity of 10 mW/cm^2). This chamber was also employed for the post-curing of the printed samples.

The 3D printer is the Asiga MAX UVX27 (*Figure 23*), it has a LED UV light source emitting at a wavelength of 385 nm. Layers can be printed within a range of $1 \text{ }\mu\text{m}$ and $500 \text{ }\mu\text{m}$ in the z-plane. The pixel resolution is $27 \text{ }\mu\text{m}$. The maximum build volume x,y,z corresponds to $51,8 \times 29,2 \times 75 \text{ mm}$ [63].



Figure 23. Asiga MAX UV X27.

The software used to prepare the models and select the various parameters for the printing phase is Asiga Composer software. It takes in input STL, SLC, PLY, STM file formats.

As explained in section 4.3, the process of creating each layer involves the vertical movement of the platform on which the inverted sample is printed. Initially, the platform approaches the bottom of the vat containing the selected formulation, leaving a space equal to the layer's thickness (approach phase). The LED light then turns on and irradiates the formulation for a set time (irradiation phase). Subsequently, the platform moves away from the vat (withdrawal phase), allowing a continuous layer of liquid formulation to form before the next approach phase.

The main parameters that were considered and consequently optimized through the printing tests are: light intensity, exposure time and layer thickness.

The first layers, which are called the burn-in layers, typically need higher exposure times to ensure that they effectively attach on the building platform. So, the optimization of the printing parameters was made considering this need, and also the effect of other parameters such as the wait time after exposure, wait time after separation and wait time after approach. These wait times are useful to allow the still-liquid resin to drain from the already printed part, to redistribute in the vat after separation of the building platform, or to prevent the formation of bubbles that can lead to defects.

After the printing phase, the final objects are post cured in the previously cited UV chamber for 3 to 5 minutes to complete the polymerization.

5.4 Characterization methods

In this chapter, the methods used to characterize the formulations listed in section 5.2 will be described. In particular, these are the assessment methods:

- Preliminary tests (material test and choice of the PI)
- FTIR-ATR spectroscopy
- Rheological analysis
- Mechanical analysis
- Swelling test and water stability

After conducting the aforementioned analyses and selecting the most suitable formulation, objects with different geometries were printed. This was done to evaluate the printing resolution and the precision of geometric features like edges, corners, and fillets. Images and considerations on these printed objects will be reported in the results and discussion section.

5.4.1 Preliminary tests

Before deciding on the final composition of the formulations, tests were conducted on two photoinitiators to select the most suitable in terms of UV light reactivity and to optimize printing parameters. These features were investigated using the printer's material test function. For this purpose, the desired resin was placed in the vat, and a circular spot (diameter 10mm) was projected; the irradiation intensity was set to 50 mW/cm² and the time was decreased sequentially from 210 to 30s. After projection, uncured resin was rinsed, and the cured film was measured at least three times using a calliper with a 0.1 mm precision. The photoinitiators considered were: lithium

phenyl-2,4,6-trimethylbenzoylphosphinate (LAP) and bis(mesityl)phosphinic acid (BAPO–OH). Specifically, material test was conducted on P3 formulations containing different photoinitiators (1% LAP and 2.5% BAPO-OH), with and without a radical scavenger, to determine if and how the scavenger influenced their curing behavior. After irradiation, each cylindrical sample is retrieved, and average thickness was measured: each thickness measurement is associated with the exposure energy, calculated by multiplying the light intensity by the exposure time. This test serves to provide an indication of the reactivity of the resins in question by correlating the degree of polymerization (thickness) with the exposure energy. In section 6.1, results of this test are reported.

Additionally, a photo-rheology test was conducted on formulations containing the 2 photoinitiators with the radical scavenger to investigate the kinetics of the photopolymerization reactions. In paragraph 5.4.4, the rheometer setup for the photorheology test is described.

5.4.2 FTIR-ATR spectroscopy

Fourier-Transform InfraRed spectroscopy (FTIR) with Attenuated Total Reflectance (ATR) is an analytical technique widely used in material research to identify and characterize materials. It measures how infrared light interacts with a material. The sample material absorbs specific wavelengths of the IR light, which correspond to the vibrational modes of the molecules in the material. By performing Fourier transform operations, the absorption data are converted into an absorption spectrum.

This spectrum presents peaks at wavelengths where the material absorbs IR light (total range 4000-500 cm^{-1}). The ATR accessory allows for the measurement of material absorption, focusing on the surface of the sample rather than its bulk (depth of analysis of about 2 μm).

Through FTIR spectroscopy, various compositions of the characterized resin were analysed. Specifically, IR spectra were obtained from samples composed of the elements listed in *Table 2*. These formulations, in which the elements were added gradually, were characterized to track changes in peaks related to functional groups that reacted or were formed.

COMPOSITION	SAMPLE FORM
DTT	powder
borax	powder
DTT + borax	powder
PEGDA	solid
HEMA	solid
PEGDA + HEMA	solid
PEGDA + HEMA + DTT	solid
PEGDA + HEMA + DTT + borax	solid
PEGDA + HEMA + DTT + borax + RS	solid

Table 2. Composition of the formulations for FTIR-ATR spectroscopy analysis.

The DTT and borax samples were tested in their natural powder form.

The DTT and borax powder was prepared by initially dissolving borax and DTT in PBS, obtaining a solution, which was then placed to evaporate in a vacuum oven at 60°C.

The other samples were prepared in PBS with 1% LAP and then printed.

The IR spectra were recorded with a FT-IR Nicolet iS50 spectrometer in ATR mode, with a resolution of 4 cm⁻¹, averaging 32 scans for each spectrum, in a wavenumbers range of 500 – 4000 cm⁻¹. As the amount of ester groups (-COOR) is constant for all samples, the spectra were normalized with respect to the 1720 cm⁻¹ peak, corresponding to this group.

5.4.3 Rheological testing

Rheological testing is crucial for understanding the flow and deformation behaviour of materials under various conditions. Features like viscosity and photo reactivity can be determined and insights into the material's behaviour under different stresses and strains can be provided. This is particularly important in developing resins for 3D printing, where the texture and processability of the resins are important features. Conducting rheological tests allows for the optimization of formulations and aids in the development of materials with desirable characteristics.

We determined the viscosity through flow curve tests and the photo reactivity through photorheology tests for the various formulations listed in *Table 1*.

An Anton PAAR Modular Compact Rheometer (Physica MCR 302, Graz, Austria) was used (*Figure 24*), configured with a parallel plate setup; the plate diameter was 25mm.



Figure 24. Anton Paar MCR 302 rheometer.

Flow curve tests on a rheometer measure the relationship between shear stress and shear rate, providing a comprehensive understanding of the resin's viscosity behaviour under different flow conditions. By analysing the flow curves, the resin's viscosity profile, shear thinning or thickening behaviour can be determined. In a flow curve, viscosity is plotted as a function of shear rate, and there are three main cases:

- Constant viscosity: Newtonian fluid
- Decreasing viscosity with increasing shear rate: Pseudoplastic fluid (shear-thinning)
- Increasing viscosity with increasing shear rate: Dilatant fluid (shear-thickening)

The parameters setting for the flowcurve tests are listed below (Table 3).

Shear rate range	0.1-5000 s ⁻¹
Temperature	25°C
Gap between plates	0.5 mm

Table 3. Parameters setting for flowcurve test.

Regarding real-time photorheology tests, these are essential for the characterization of photo reactivity and mechanical properties of the photocurable resins. During this test, the time evolution of the storage modulus (G') and the loss modulus (G'') are evaluated, while maintaining constant oscillation amplitude and frequency over time. These tests involve exposing the resin to a UV light source (activated at a certain instant) while simultaneously measuring its G' and G'' over time. The storage modulus (G') and the loss modulus (G'') are two quantities that describe the viscoelastic

behaviour of a polymeric material. G' describes the elastic component of the material's response to deformation, whereas G'' describes the viscous component. Typically, when the material is in its liquid form, $G'' > G'$, and when it is solid, $G' > G''$. Through this test, it is possible to observe how the resin's behaviour changes during the curing process, providing insights into the kinetics of polymerization and the final mechanical properties of the cured material.

In photorheology, some important parameters must be considered, such as the gel point, delay time, final G' , and total reaction time. Moreover, the slope of the G' and G'' curves are important since they indicate how quickly the material's rheological behaviour is evolving as it undergoes polymerization or cross-linking. In section 6.3.2, these factors are presented for each type of tested resin and have contributed to the selection of the optimal formulation for DLP 3D printing.

For the real-time photorheology tests, the UV-light source was provided by positioning the light guide of the UV Hamamatsu LC8 lamp (emission at 365 nm) under the bottom plate. A quartz glass plate was employed in the rheometer setup to ensure transparency to incident UV radiation. The light source was positioned at 70 mm from the quartz plate, and the lamp intensity was set to 100%. During the measurements the sample was kept under a constant shear frequency of 1 Hz. The irradiating light was switched on after 60 s to allow the system to stabilize before the onset of polymerization. According to the preliminary amplitude sweep measurements (described below), all the tests were carried out in the linear viscoelastic region at a strain amplitude of 50%.

In *Table 4*, the process parameters for the conducted photorheology tests are reported.

Gap between plates	0.5 mm
Temperature	25°C
Oscillation amplitude	50 %
Oscillation frequency	1 Hz
Time between two consecutive measures	1 s
UV lamp ON at	60 s

Table 4. Photorheology process parameters.

Amplitude sweep test is performed to determine the linear viscoelastic region (LVE) of the resin. During this test, the upper plate applies sinusoidal stress to the sample, characterized by a constant frequency and variable amplitude within a certain range. The amplitude sweep helps identify the strain range in which the material exhibits linear viscoelastic behavior, meaning that the G' remains constant regardless of the deformation applied. This information is crucial for ensuring that subsequent rheological measurements, including photorheology tests, are conducted within this

linear region to obtain accurate and reliable data. In *Figure 25*, an example of the results of an amplitude sweep test is reported, where the LVE region is before the strain limit γ_L .

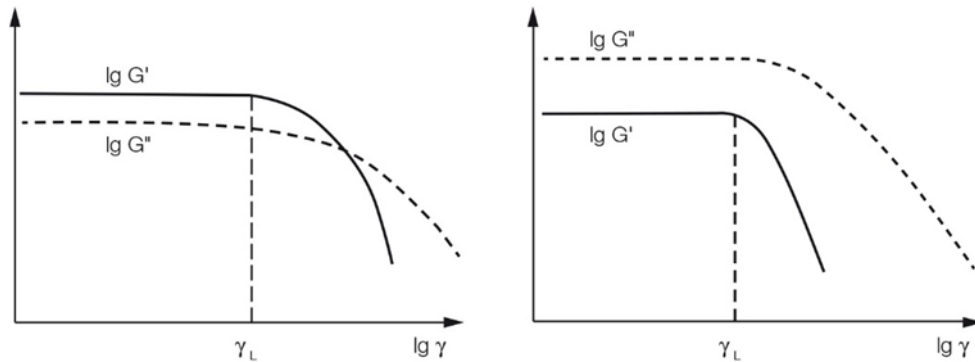


Figure 25. Example of an amplitude sweep test results representation.

Here, amplitude sweep tests were performed in the range of 1 to 1000% strain, with a frequency of 1 Hz. In *Table 5*, all the process parameters for the amplitude sweep test are reported.

Gap between plates	0.5 mm
Temperature	25°C
Oscillation amplitude range	1-1000 %
Oscillation frequency	1 Hz
N° of measures	30

Table 5. Amplitude sweep process parameters.

5.4.4 Mechanical testing

Mechanical testing is essential in materials science as it provides critical insights into the behaviour and performance of materials under different types of loads and stresses. Understanding the mechanical properties of materials is fundamental for predicting their performance and to characterize their response to various stresses.

In this study, we conducted tensile and compression tests on various formulations. These tests are crucial for evaluating key mechanical features such as elastic modulus, which indicates the stiffness of the material, and elongation at break, which measures its ductility. Additionally, assessing the self-healing efficiency of these materials is crucial for determining their suitability for applications where the ability to self-repair after damage is needed. By characterizing these properties, we aimed to identify the formulations with the best combination of mechanical performance and self-healing capabilities.

For both tensile and compression tests a Z3 tensile tester (AML Instruments) with a 500 N load cell equipped with tensile and compression grippers was used. The data were generated and collected using THSSD software.

5.4.4.1 Tensile test

Tensile testing is a fundamental method used to assess the mechanical properties of materials; it provides information on the material's strength, elasticity, and overall performance under tension. The purpose of tensile testing is to evaluate the material's ability to withstand stretching forces, which is crucial for applications where the material will be subjected to tension. Through this test, we were able to obtain stress-strain curves. The stress is the force per unit area, while the strain is the deformation relative to the initial length. This test was performed to evaluate the effectiveness of the self-healing mechanism. By subjecting the hydrogel to multiple cycles of tensile loading, damage, and subsequent healing, the recovery of mechanical properties was assessed.

The analyzed mechanical features are:

- Elastic Modulus: it represents the stiffness of the hydrogel; it is calculated from the slope of the initial linear portion of the stress-strain curve.
- Ultimate elongation at break: it's the value of the strain at the breaking point.

The hydrogel samples were dog-bone shaped and were printed with the same dimensions, represented in *Figure 26*.

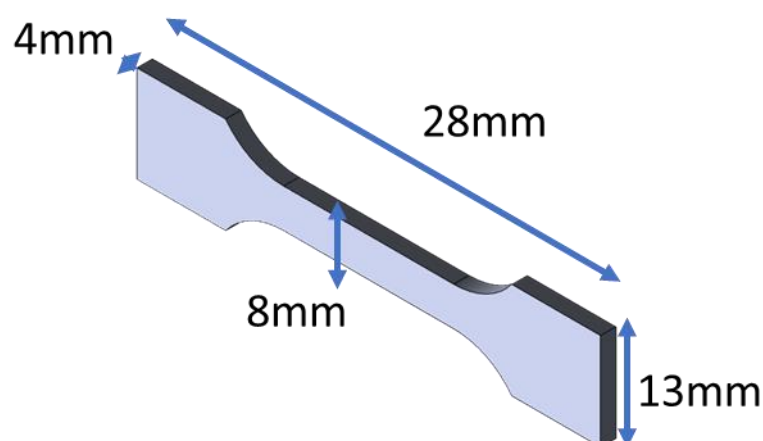


Figure 26. Dimensions of the samples for tensile test.

Since at the end of the preparation of formulations B1 and B2 they spontaneously gelled multiple times, they were not considered and therefore the related samples were not printed. It is noted that

formulations B3 and P3 coincide. For reasons of statistical reliability, printer availability, and printing times, it was decided to print and test samples related to formulations P1, P3, P5, and B5.

In *Table 6*, the number of samples produced for each formulation type is reported. The exposure times for the 3 burn-in layers and the remaining layers are also provided. Light intensity was set at 50 mW/cm² and the layer thickness was 70 μm for every printed sample.

FORMULATION NAME	Texp burn-in layers [s]	Texp other layers [s]	N° OF SAMPLES
P1	55	45	6
P3	35	28	9
P5	35	28	7
B5	28	24	8

Table 6. N° of samples and relative formulation type for tensile test with their exposition times.

After fracturing the samples, the two parts were repositioned to align their surfaces as closely as possible to facilitate the self-healing process. The samples were kept in sealed petri dishes covered with Parafilm along with wet paper soaked in deionized water to maintain a minimum level of humidity and prevent them from drying out. The samples were re-tested through several cycles of self-healing resulting in stress-strain curves for the self-repaired samples. This allowed for the evaluation of the recovery of the considered mechanical features in percentage terms. The percentages of mechanical recovery were calculated for each sample over 3 self-healing cycles, relative to the initial value of the corresponding mechanical feature. To associate the recovery capabilities of the samples with the formulation type, an average of these recovery values was calculated across all samples for each formulation. After each self-healing cycle, the dimensions of the samples were remeasured to determine area and length, necessary for calculating the new stress-strain curves. The speed in all tensile tests was set to 5 mm/min.

In addition to the mechanical characteristics, the efficiency of self-healing was also considered, as not all samples were consistently able to self-repair during the various cycles, and tensile testing could only be repeated for some. Specifically, 3 cycles of self-healing were conducted. The timings of these cycles are reported in *Table 7*.

SH cycle 1	4 days
SH cycle 2	6 days
SH cycle 3	5 days

Table 7. Duration of the self-healing cycles performed in tensile test.

5.4.4.2 Compression test

Compression testing provides data on the sample's mechanical performances under compressive loads. This is important for applications where the material must withstand compressive loads, such as in tissue engineering and soft robotics.

The tested samples' shape and dimensions are depicted in *Figure 27*.

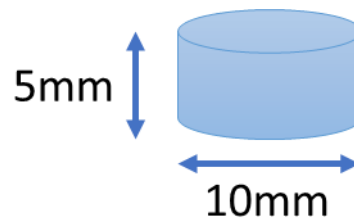


Figure 27. Sample dimensions for compression test.

The printed samples were stored similarly to those mentioned earlier used for tensile testing. The compression behaviour of the samples from various formulations was qualitatively evaluated by observing the state of the samples during the test and upon completion.

In *Table 8* the number of the tested samples is reported.

FORMULATION NAME	N° OF SAMPLES
P1	4
P3	6
P5	4
B5	4

Table 8. N° of samples and relative formulation type for compression test.

Due to the destructive nature of the test, (the samples were shattered into many small fragments at the end of the test) no self-healing cycles were performed, and the compression analysis was limited to evaluating the condition of the various samples after the test.

The process parameters for the compression test are reported in *Table 9*. The initial displacement was set as the specific sample thickness minus 0.4 mm. For P1, due to its wider elongation range, the displacement was set as the sample thickness minus 0.2 mm.

Speed	3 mm/min
Pre Load	0.1 N
Maximal Load	100 N
Displacement	S – 0.4 mm

Table 9. Parameters setting for compression test.

5.4.5 Swelling test

Swelling tests on printed hydrogel samples offer insights into their water absorption capabilities and structural stability in aqueous environments. Given that this ability is similar to that of the extracellular matrix, it is important to consider if the applications of the hydrogel fall into tissue engineering, wound dressings, and drug delivery. The key parameters that need to be analysed in this type of test are:

- Swelling ratio: it indicates how much water the hydrogel can absorb relative to its dry weight. It was calculated with the following formula, where W_t is the weight of the swollen hydrogel at time t and W_o is the initial dry weight.

$$Q (\%) = \left(\frac{W_t - W_o}{W_o} \right) * 100$$

- Equilibrium swelling: it is the swelling ratio value at which the hydrogel is fully saturated.
- Swelling kinetics: it expresses the rate at which the hydrogel absorbs water and reaches equilibrium.

As the P3 was the optimal formulation in terms of mechanical properties, self-healing capability and printability, swelling test was performed only on this formulation.

The hydrogel was weighed at the time steps reported below (*Table 10*).

SWELLING TEST TIME STEPS
10 min
20 min
30 min
1 h
2 h
24 h

Table 10. Swelling test time steps.

6. Formulations Characterization: Results and Discussion

In this chapter, the experimental results obtained from the characterization of photocurable resin formulations for 3D printing self-healing hydrogels via DLP are presented. The initial experiments were designed to choose the most suitable photoinitiator for an optimal printing process. The chemical composition of the resin elements and different printed hydrogels was investigated using FTIR-ATR spectroscopy. Furthermore, the mechanical and rheological properties, curing behavior, and self-healing efficiency of the resins were evaluated under different conditions. These tests were conducted on various formulations, differing in DTT-borax ratio and DTT-acrylate ratio (listed in *Table 1*), to study these properties and select the optimal formulation in terms of mechanical properties recovery and 3D printing requirements.

6.1 Preliminary tests

Initially, in order to choose the optimal photoinitiator for determining the final composition of the photocurable resin formulation and to optimize the printing process, material tests and photorheology were conducted on four formulations containing LAP and BAPO-OH as photoinitiators, both with and without radical scavenger. The quantities of the other elements present in the tested resins correspond to those of the P3 formulation (section 5.2).

Regarding the material test, the exposure times selected using the material test function integrated into the printer are shown in *Table 11*.

EXPOSURE TIMES [s]			
BAPO NO RS	BAPO RS	LAP NO RS	LAP RS
		30	30
45	45	45	45
60	60	60	60
90	90	90	90
120	120	/	/
150	150	/	/
180	180	/	/
210	210	/	/

Table 11. Exposure times set for material test.

Recalling that the light intensity was set to 50 mW/cm², by multiplying this by each exposure time, the respective exposure energy to which the resins were subjected during the test was calculated. In order to evaluate how much time a formulation takes to polymerize when exposed to the calculated exposure energies, the relationship between thickness and exposure energy was plotted, and a linear fitting was performed for the various formulations (*Figure 28*).

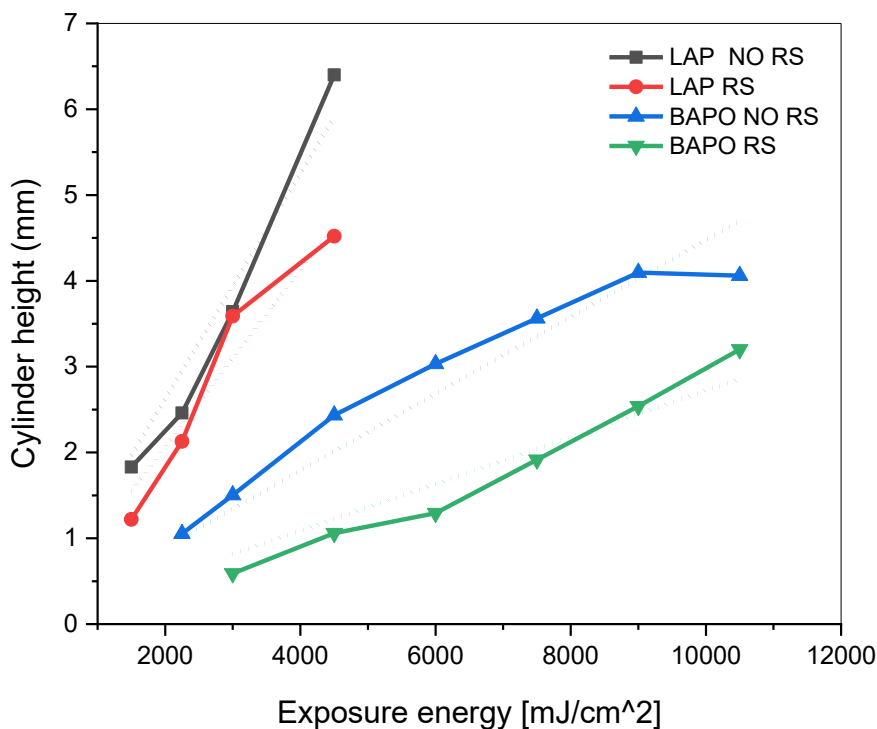


Figure 28. Material test.

Through the analysis of these data, it is possible to compare these formulations in terms of UV light reactivity. It can be observed that formulations containing BAPO-OH exhibit slower polymerization reactions compared to those containing LAP, resulting in products with thicknesses of 4-5 mm being obtained in considerably longer times. Given this, formulations with LAP were only tested for exposure times up to 90 seconds. Regarding the presence of the radical scavenger, comparing the linear trends of both types of formulations, it appears to influence them by slightly slowing down polymerization. Obtaining samples of lower thickness at equal exposure energies suggests that its antioxidant effect reduces the polymerization rate of the resins. Therefore, it may be useful to integrate it into the resin to control the degree of polymerization, assessing its effect on the printing process. To further evaluate the resins photoreactivity and the reaction kinetics, photorheology tests were also performed on both formulations containing LAP and BAPO-OH with radical scavenger (*Figure 29*).

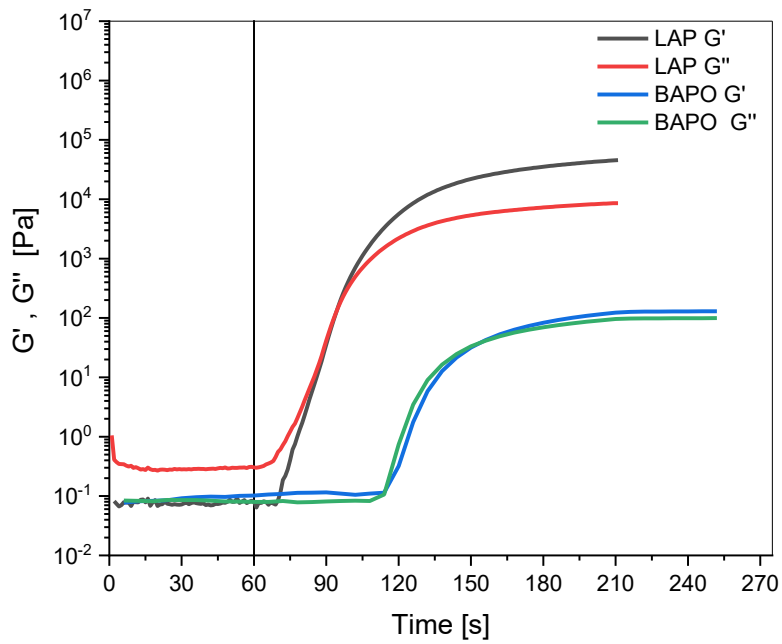


Figure 29. Photorheology test.

It is further confirmed that BAPO-OH as a photoinitiator leads to slower polymerizations, requiring more time to complete. In addition to having a longer latency time, it also results in significantly less rigid products compared to those obtained with LAP (the final G' moduli differ by approximately 2 orders of magnitude). Moreover, the total reaction time of the formulation with LAP is shorter. Regarding the time needed to reach the gel point, it is almost identical. These data are reported in Table 12.

	LAP	BAPO-OH
Delay time	10 s	54 s
Total reaction time	100 s	150 s
Final G'	45 600 Pa	130 Pa
Gel-point time	30 s	30 s

Table 12. LAP and BAPO-OH photorheology most relevant data.

Analyzing these preliminary results, the choice of photoinitiator fell on LAP because, being more reactive to UV light and leading to faster and more effective polymerizations, it allows for printing objects in significantly shorter times compared to those required when using BAPO-OH.

6.2 FTIR-ATR spectroscopy

To study the chemical composition of the various elements of the resin and evaluate how they interact to form the final hydrogel, infrared absorption spectra of the species listed in Table 2 in section 5.4.2 of Materials and Methods were obtained. Initially, the absorption spectra of DTT, borax, and DTT + borax were obtained. The following considerations were made for these spectra:

DTT: The OH groups in the structure can be related to the two peaks found between 3225 and 3375 cm^{-1} . The peaks present between 2600 and 2550 cm^{-1} are assigned to the stretching vibration of thiol SH groups (*Figure 30A*) [28].

In the range between 700 and 600 cm^{-1} , we found a peak at 675 cm^{-1} that represent the stretching vibration of C-S groups, found also in the DTT+borax spectrum (*Figure 30B*) [64].

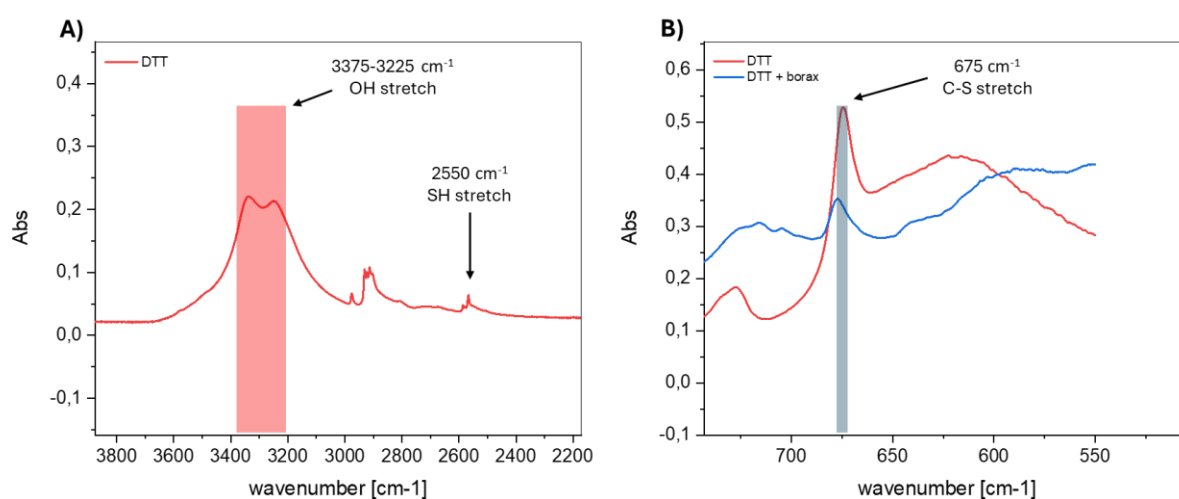


Figure 30. (A) Significant peaks in DTT absorption spectrum, (B) C-S stretching vibration peaks found in DTT and DTT + borax spectra.

BORAX: The signals due to the asymmetric stretching of the B-O bonds in BO^3 and BO^4 are found at 1350 cm^{-1} and between 1120 and 1065 cm^{-1} , respectively. Also, the peak at 830 cm^{-1} can be ascribed to the stretching of the B-O groups of the tetraborate ion $\text{B}(\text{OH})_4^-$ (*Figure 31*). [65]

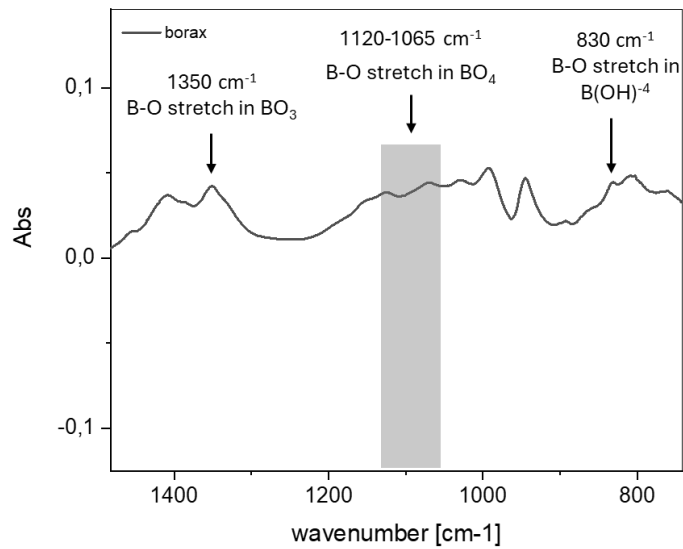


Figure 31. Significant peaks in borax absorption spectrum.

DTT + BORAX: at 2550 cm⁻¹ we can find a peak, as in DTT spectrum, that is related to the stretching vibration of SH groups [28]. Boronate ester bonds formation can be attributed to the signals in the band region between 1400 and 1300 cm⁻¹, representing their characteristic vibrational mode (Figure 32) [66].

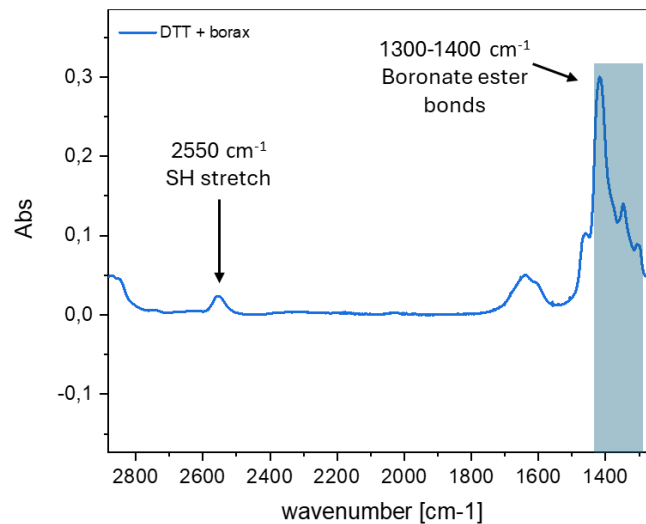


Figure 32. Significant peaks in DTT + borax absorption spectrum.

This is an interesting result since, in the initial part of the resin preparation procedure, DTT-borax complexes are intended to be formed, creating compounds with boronate ester bonds with terminal thiol (SH) groups. In this way, these complexes can react via thiol-ene reaction between the SH

groups and the C=C double bonds of acrylates, integrating the DTT into the polymeric network chains, which will be connected by boronate ester bonds.

Regarding the other tested samples, we started with PEGDA and HEMA alone, then gradually added the other elements until the final hydrogel was obtained. It should be noted that since the addition of the radical scavenger does not alter the absorption spectrum of the hydrogel, the following graphs will show the final hydrogel labelled as P+H+D+B.

PEGDA: in this spectrum, PEGDA characteristic carbonyl groups and C=C bonds signals can be found respectively at 1729 cm^{-1} and between 1650 and 1630 cm^{-1} (Figure 33). [67]

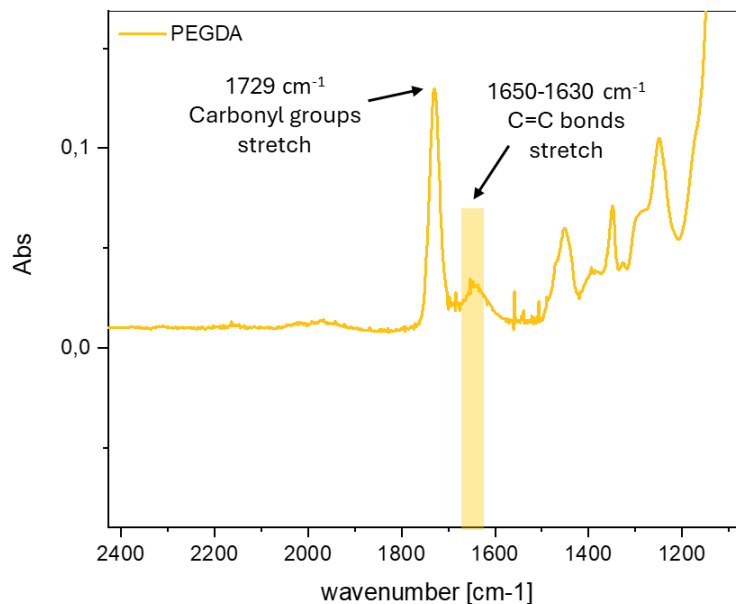


Figure 33. Significant peaks in PEGDA absorption spectrum.

HEMA: in HEMA absorption spectrum we found OH groups stretching vibration signals in the band between 3200 and 3600 cm^{-1} . At 1720 cm^{-1} the signal represents the stretching vibration of carboxylic ester groups. Moreover, in the 3000 - 2800 cm^{-1} band the CH stretching signals of the methyl groups (CH_3) and methylene groups (CH_2) can be attributed to these peaks (Figure 34). [68]

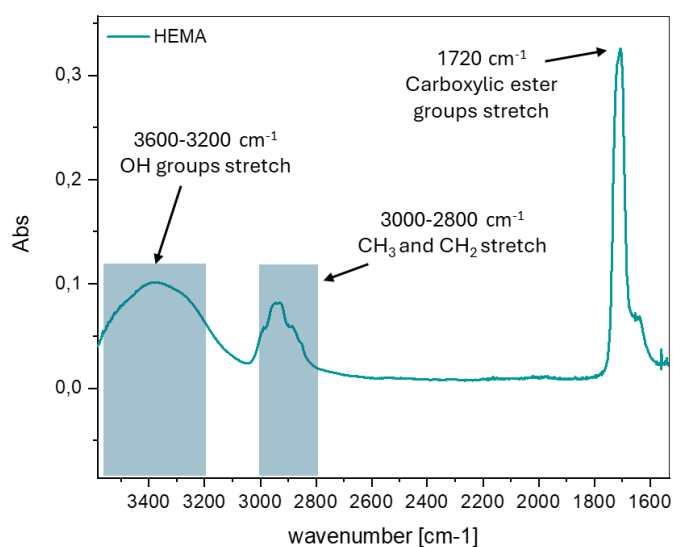


Figure 34. Significant peaks in HEMA absorption spectrum.

Comparing the spectra with an increasing number of ingredients, it is important to note that the signal due to the presence of SH groups (present in the spectra of DTT and DTT+borax) is not present in any sample. While this is obvious in P+H sample, this absence in the other spectra suggests that the S-H groups have reacted with the acrylates and now become part of the polymeric network (Figure 35A and 35B).

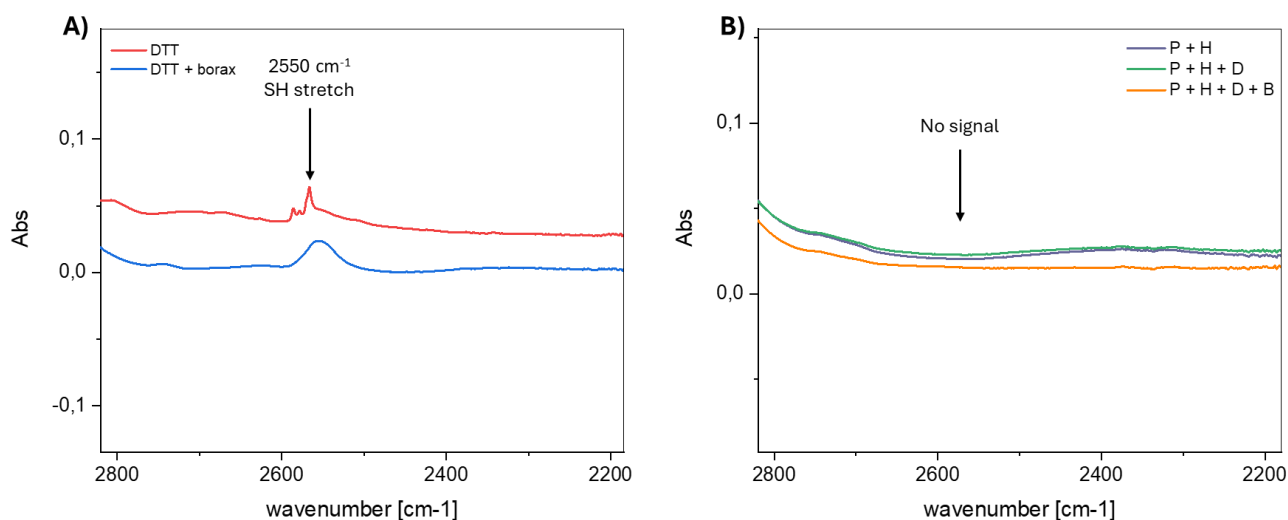


Figure 35. (A) SH groups stretching signal in DTT and DTT + borax spectra, (B) acrylates and final hydrogel spectra.

Another interesting observation can be made by comparing the spectra shown in Figure 36, where peaks at 705 and 680 cm^{-1} are evidenced in the final hydrogel. These can be attributed to the presence of C-S and B-O bonds, respectively [65].

Furthermore, in the band between 1450 and 1350 cm^{-1} , an increase in signal intensity can be observed, which can be attributed to the stretching of the O-B-O bonds in the boronate ester bonds (Figure 36A and 36B) [69].

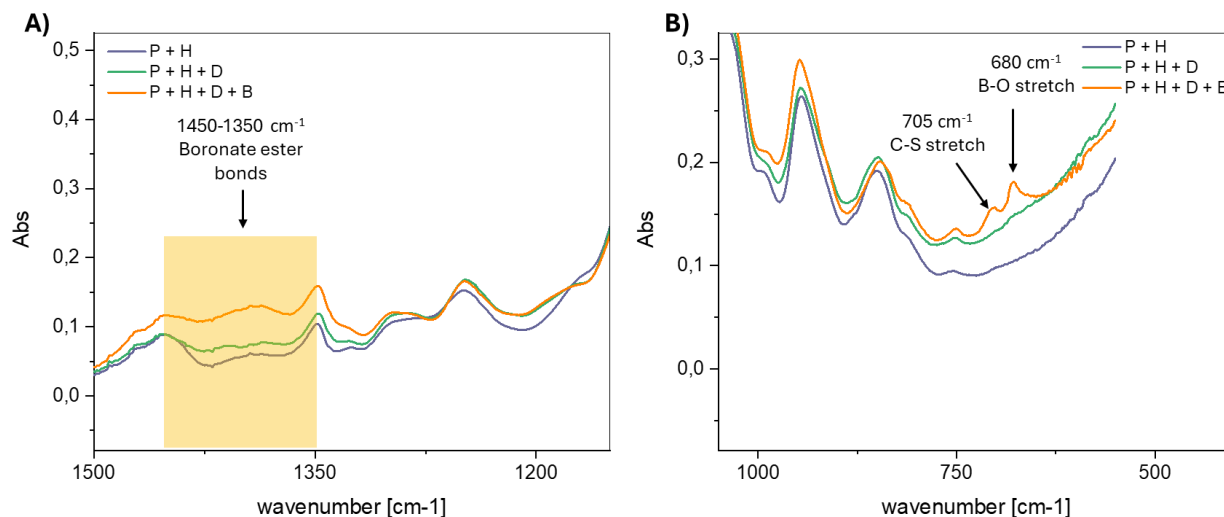


Figure 36. (A) O-B-O stretching band slightly increased in signal in final hydrogel, (B) C-S and B-O bonding signals in final hydrogel.

Considering the values corresponding to the absorption bands and peaks found in literature and compatibly studying the experimentally obtained spectra, the results suggest that in the final hydrogel, DTT-borax complexes have been well integrated into the polymeric structure.

6.3 Rheological analysis

To characterize the rheological properties of the different formulations listed in Table 1, rheological measurements were performed. Specifically, flow curves were obtained to evaluate viscosity as a function of shear rate, and photorheology was conducted to characterize viscoelastic properties and assess gelation kinetics of the different formulations. This was done to investigate how the various ratios of ingredients constituting the hydrogel influence these properties.

Regarding formulations B1 and B2 (listed in Table 1), these were excluded a priori from the various characterization tests because they spontaneously gelled upon preparation, making impossible to test them. It is noted that formulations B3 and P3 are identical.

6.3.1 Viscosity

The flow curves of the various formulations are shown in *Figure 37*. The P formulations trend indicates that the presence of borax slightly influences the resin's viscosity. B formulations, which contain higher amounts of acrylates, exhibit a more pronounced shear-thinning behavior compared to the P formulations. Overall, all formulations show viscosity ranges suitable for DLP 3D printing.

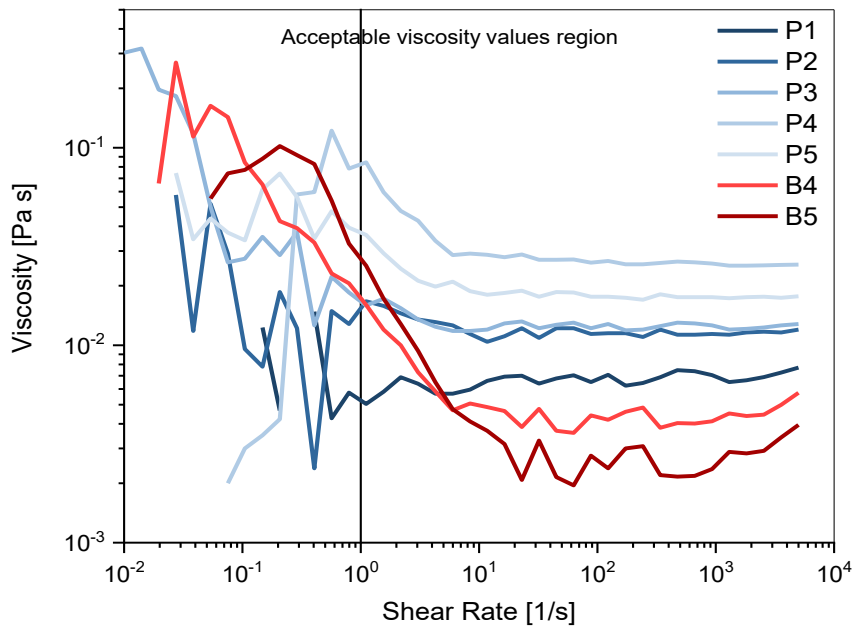


Figure 37. P and B formulations flowcurves.

To evaluate the viscosity trends, values of shear rate equal to or greater than 1 are considered, as in the preceding range we encounter torque values below $0.01 \mu\text{m}$, which are close to the sensitivity limit of the rheometer. Therefore, viscosity values measured in the shear rate range between 0.01 s^{-1} and 1 s^{-1} are not reliable. The trend of torque as a function of shear rate is shown in the *Figure 38*.

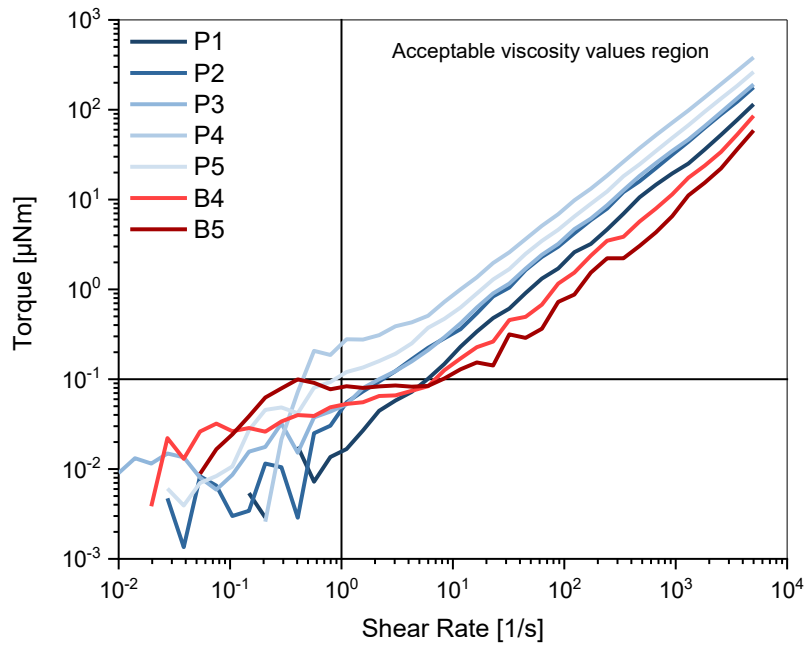


Figure 38. Torque in function of shear rate during flowcurve test.

6.3.2 Photorheology

According to the preliminary amplitude sweep measurements, all the tests were carried out in the linear viscoelastic region at a strain amplitude of 50% as explained in section 5.4.3. The UV light positioned under the samples was turned on 60 seconds after the start of the measurements to allow the samples to stabilize before polymerization began. The evolution over time of the storage modulus (G') was plotted for each formulation to compare parameters such as final G' , slope of the curves, latency times, and others. The results of the photorheology tests are shown in *Figure 39*.

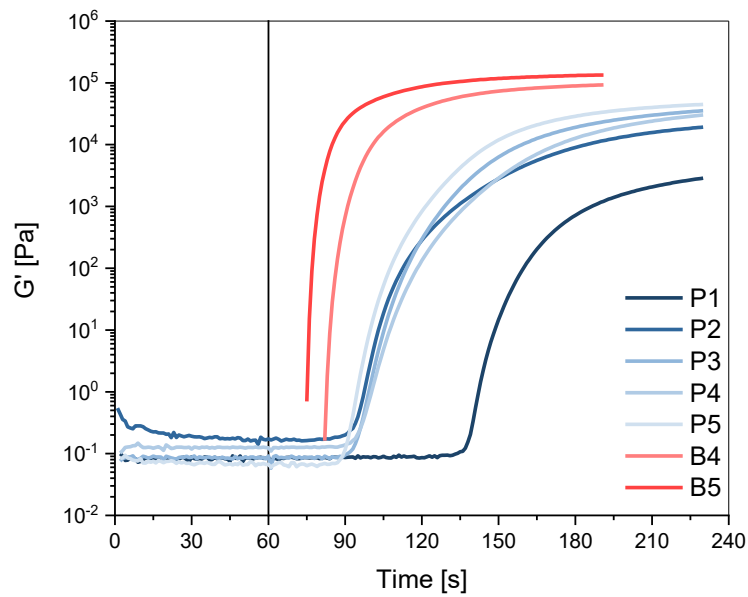


Figure 39. Time evolution of G' in photorheology tests of P and B formulations.

Regarding the curves of formulations B4 and B5, due to technical reasons, it was not possible to measure the storage moduli (G') before the start of polymerization. Therefore, for comparison purposes, only the slope of the curve and the final G' modulus of the samples were evaluated. From the graph, it can be observed that formulation P1, containing more borax, exhibits a longer latency time compared to the others and a lower final G' modulus. On the other hand, the other P formulations show nearly similar behaviors among them. Increasing the acrylates in the resin (B4 and B5) resulted in stiffer final products (G' on the order of 10^5 Pa) and faster reactions. Given the highly reactive nature of acrylates, this outcome was expected as their chains undergo free radical chain polymerization reactions more readily. P formulations (where acrylates:DTT = 2:1) are characterized by longer reaction times and slower polymerization rates. This result is attributed to the higher content of DTT in these formulations. During polymerization, DTT and acrylates react via thiol-ene reaction (a radical step-growth polymerization type), which slows down the overall reaction time for the P formulations. The resulting products will be less rigid and will require longer printing times compared to the B formulations. However, with more DTT integrated into the polymer chains, these formulations possess more functionalities to enable self-healing properties.

By individually analyzing the curves (Figure 40) and examining the trends of the storage modulus (G') and loss modulus (G''), significant data regarding total reaction time, latency time, time to reach

the gel point, and final G' modulus for each P formulation were extracted and are reported in *Table 13*.

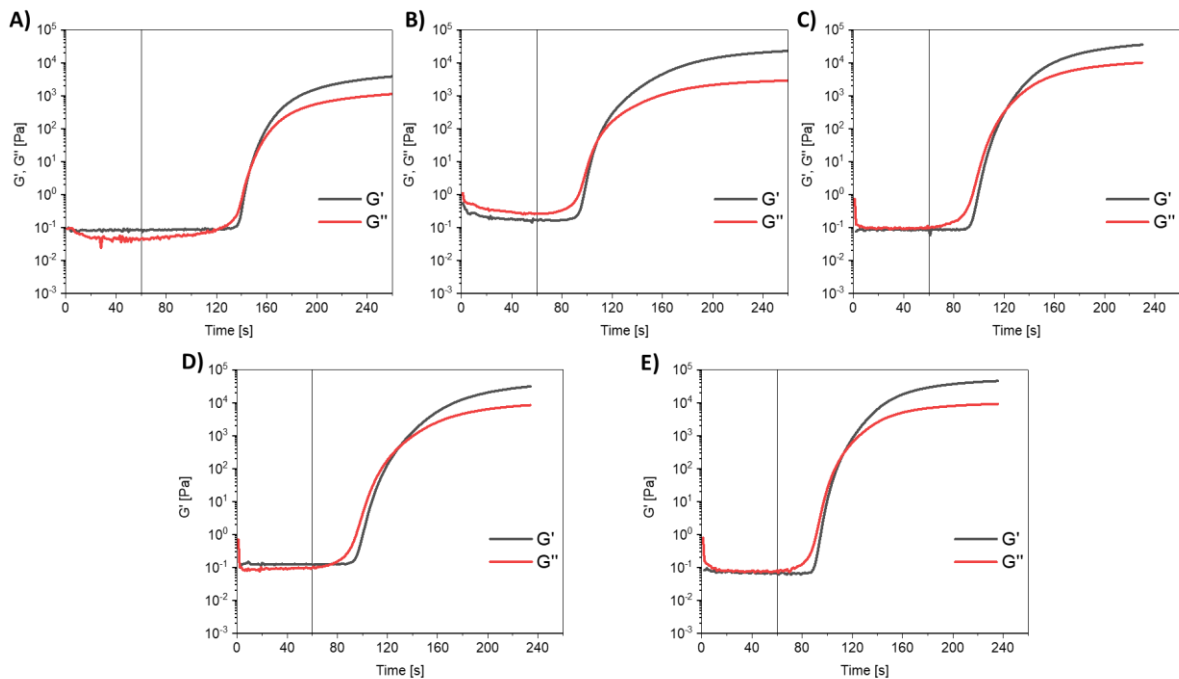


Figure 40. Photoreology curves of formulation: (A) P1, (B) P2, (C) P3, (D) P4 and (E) P5.

	Delay time	Total reaction time	Time for reaching gel-point	Final G'
P1	76 s	124 s	11 s	3,85 kPa
P2	32 s	148 s	16 s	20,5 kPa
P3	31 s	134 s	29 s	35,4 kPa
P4	30 s	140 s	38 s	31,3 kPa
P5	28 s	142 s	25 s	45,9 kPa
B4	/	/	/	99,1 kPa
B5	/	/	/	134 kPa

Table 13. Data extracted from photoreology curves of P and B formulations.

Examination of these data reveals a mild trend: decreasing the amount of borax results in slightly stiffer products. This can be justified by the fact that a higher presence of borax within the network can impart flexibility to the polymer chains. As above mentioned, formulation P1 shows significant

delay compared to the other formulations, which instead show very similar latency times, around 30 seconds. The total reaction times do not differ significantly among the P formulations.

6.4 Mechanical analysis

In order to study how the mechanical properties of the samples vary based on different ratios between DTT and borax, and between acrylates and DTT, formulations P1, P3, P5, and B5 were tested. These formulations were chosen due to reasons related to statistical reliability (it was preferred to print more samples related to fewer formulations rather than the opposite). Despite only four formulations being tested, given the ratios that characterize them, they well represent the variability in the quantities of the elements that compose them.

6.4.1 Tensile test

Tensile tests were conducted on dumbbell-shaped specimens, which were subjected to three cycles of self-healing to evaluate the ability to recover mechanical properties over multiple cycles, as well as their self-healing efficiency. Through this assessment, it was possible to identify the optimal formulation in these terms. The dimensions of these samples, the printing parameters used to produce them, and the duration of the three self-healing cycles are reported in section 5.4.4.1. In *Figure 41* is shown an example of the tested specimens printed using P3 resin.



Figure 41. Dogbone sample for tensile testing.

Considering the three self-healing cycles to which the samples were subjected, the number of specimens that effectively self-healed and consequently could be retested for each cycle was taken into account. *Figure 42* shows a histogram where the number of self-healed specimens is reported for each cycle; at cycle 0, we find the initial number of samples for each formulation.

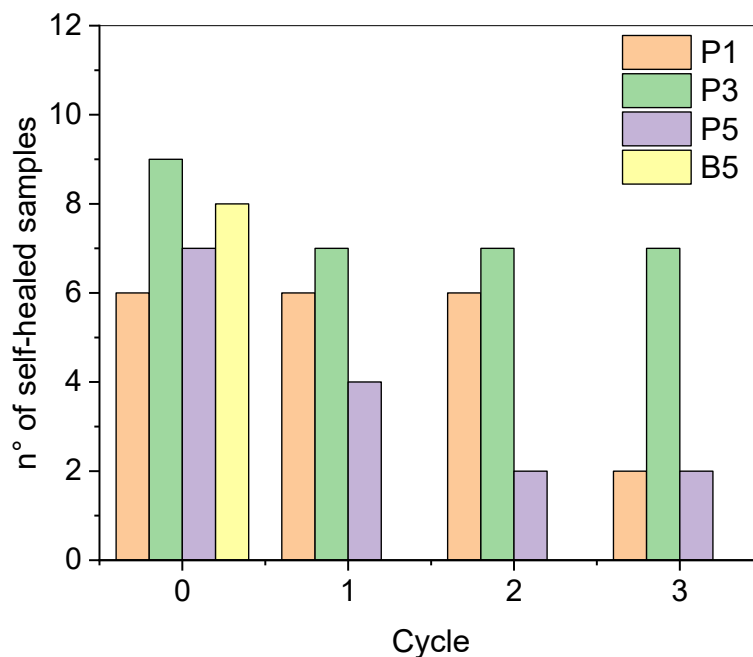


Figure 42. Number of self-healed samples per cycle.

It can be observed that B5, a formulation containing high quantities of acrylates relative to DTT, has zero self-healing efficiency starting from the first cycle. This result was expected because, given the high presence of acrylates, the sample is very rigid compared to the others and the polymer network chains have limited mobility. In fact, B5 samples underwent brittle fractures, withstanding low percentage deformations in elongation (on average 20%). Regarding P5, the samples produced with this formulation showed low self-healing efficiency: starting from the second cycle, it was possible to handle without breaking and retest only 2 out of 7 samples. The low self-healing yield of P5 samples can be attributed to the low presence of borax in the resin which is not in sufficient quantity to allow the polymer chains to reconnect through the establishment of boronate ester bonds.

Regarding P3 and P1, these demonstrated excellent self-healing efficiency, allowing the samples related to these formulations to be easily handled and retested without particular complications. As for P1, after the second self-healing cycle, it was possible to test only 2 out of 6 samples, not because the two fracture surfaces had not joined, but because they shrank and deformed to such an extent that their geometry was significantly altered, making further testing impossible. This condition can be attributed to the plastic deformation, which was observed in this sample due to low mechanical performance.

The mechanical features for which the percentage recovery was evaluated after the self-healing cycles are the elastic modulus (E) and the maximum deformation in percentage elongation at break (UEAB). The recovery percentages were calculated with respect to the initial cycle.

Figure 43A and 43B show, respectively, the average values of elastic modulus calculated on the various samples subjected to the first break and after the various self-healing cycles, and the percentage recovery of these, averaging the recoveries relative to individual samples. Columns marked with an asterisk refer to values obtained through only 2 samples. Therefore, they have low statistical significance, but it was decided to report them anyway.

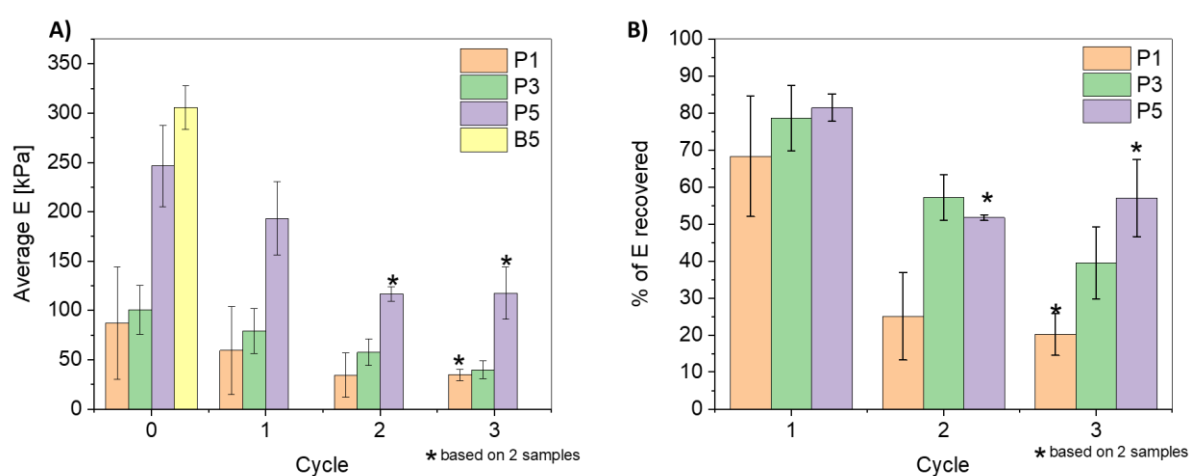


Figure 43. Average E and its % recovery performed by the hydrogels during SH cycles.

Similarly, the average values of UEAB and its mean percentage recovery for each formulation during the various cycles are reported in Figure 44A and 44B. The high standard deviation of the results can be associated with factors that commonly affect the preparation of polymer-based compounds, whereby the variability in sample behaviour increases due to factors such as: environmental factors (temperature and humidity), grip and alignment of the samples during the test, aging (it was not possible to print all samples in a single day), intrinsic heterogeneity that polymers may have at the molecular level. All these factors contribute to variability in mechanical properties of the samples. Obviously, efforts were made to proceed in the same manner for each sample in preparation, storage, and testing conditions.

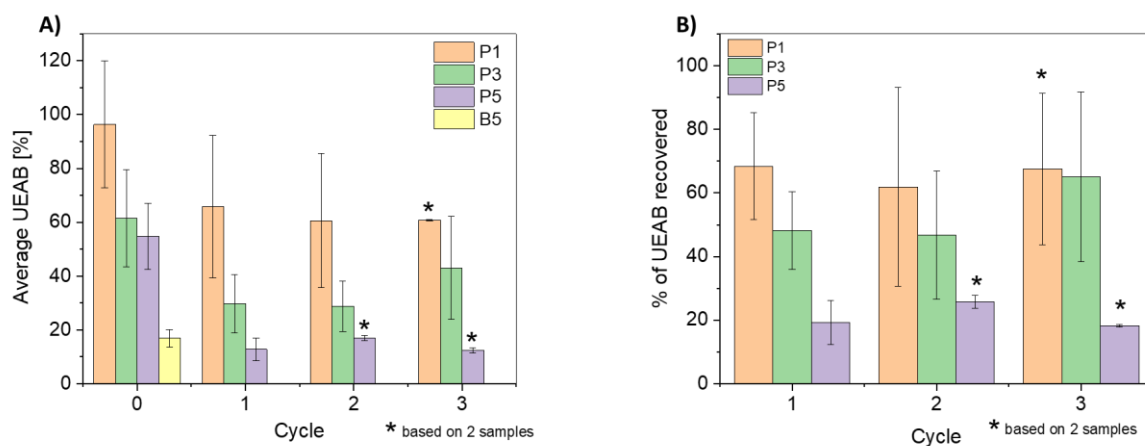


Figure 44. Average UEAB and its % recovery performed by the hydrogels during SH cycles.

Regarding the first break, it can be noted that P5 and B5 have the highest elastic moduli. The high stiffness value of B5 samples is associated with the high quantity of acrylates present in this resin. This gives B5 samples a brittle fracture behavior, a low UAEB, and no testable samples starting from the first self-healing cycle (Figure 45A). The poor self-healing efficiency is attributed to the fact that DTT and borax are present in very low quantities compared to PEGDA and HEMA.

The P5 high stiffness is probably due to the low amount of borax present in the resin. It is thought that this leads to less chain flexibility due to fewer inter-chain dynamic covalent bonds. As a consequence, the specimens have a more brittle fracture behavior, with low percentage recoveries of UEAB (Figure 45B). Moreover, the stiffness of P5 may also be due to a higher crosslinking density and a greater number of hydrogen bonds, since there are more DTT chains with the 2 exposed OH groups not bound to borax, which is present in smaller quantities compared to other formulations.

Comparing the representative stress-strain curves of the studied formulations, P5 and B5 prove to be more resistant than P1 and P3, with initial Ultimate Tensile Strength (UTS) values of about 40-50 kPa. P1 and P3 samples, instead, are able to withstand lower stresses before breaking, in the order of 10 kPa at the first break and a few kPa after self-healing. Although these values are considered low when compared to structural materials, hydrogels with these UTS can be used in TE to produce supports for cell growth. This is because these materials do not necessarily have to withstand high loads but must be biocompatible and mimic soft tissues.

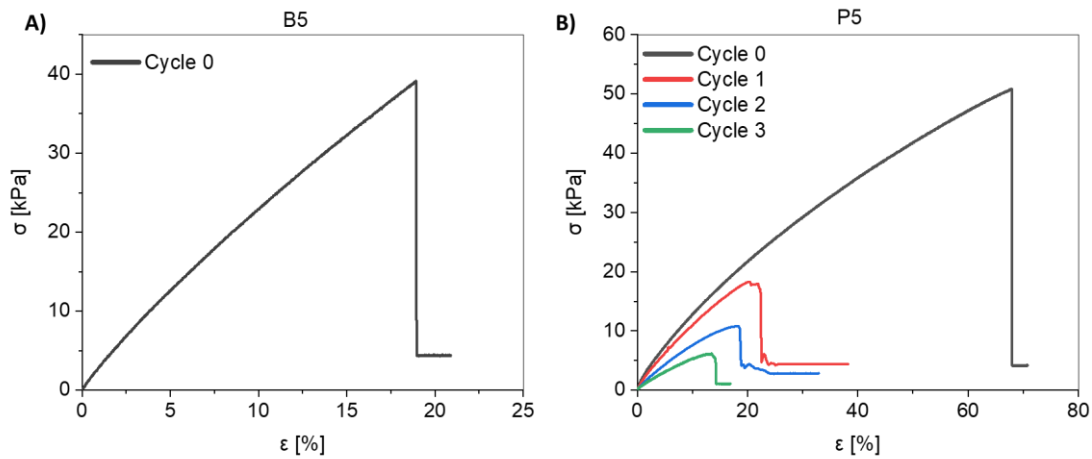


Figure 45. (A) B5 representative stress-strain curve, (B) P5 representative stress-strain curves for every cycle.

Referring to formulations P1 and P3, these are found to have a lower elastic modulus than the previous ones, but, as can be seen from the presented data, with significantly better performance in terms of self-healing, UEAB, and recovery of mechanical properties compared to B5 and P5. P1 samples are characterized by an excellent ability to recover UEAB (on average 60-70%). However, from the second cycle, the recovery of the elastic modulus is equal to low percentage values (20-30%). The good UEAB recovery of P1 can be observed in *Figure 46*, in which its representative stress-strain curves are reported.

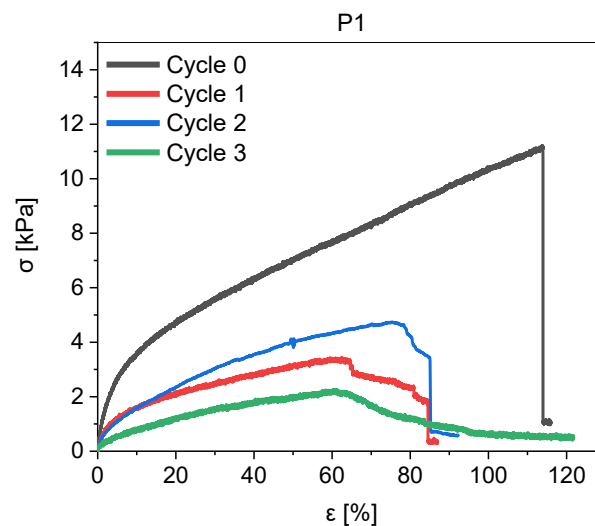


Figure 46. P1 representative stress-strain curves for every cycle.

Regarding P3, the samples printed with this formulation have excellent self-healing efficiency. In addition to this, during the three self-healing cycles, they were able to recover part of the initial elastic modulus and UEAB optimally compared to the others. Elastic modulus recovery values were obtained ranging from 80% after the first self-healing cycle, reaching 50% after the third. As for UEAB

recovery, on average after each cycle, the samples recovered 50% of the value relative to the first break. In *Figure 47*, the P3 representative stress-strain curves are reported.

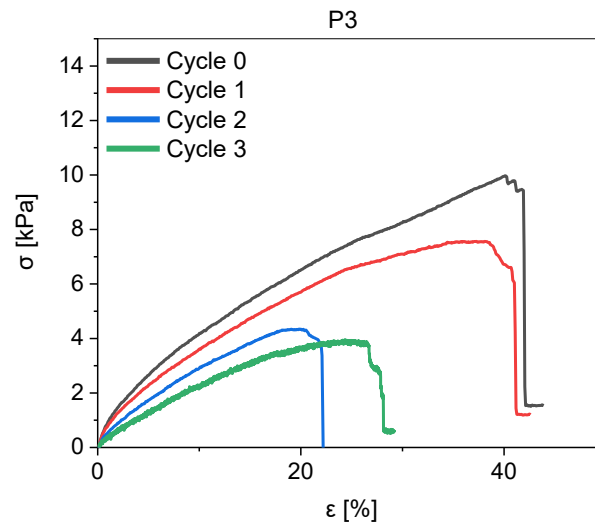


Figure 47. P3 representative stress-strain curves for every cycle.

Given this, P3 proves to be the optimal formulation with the best performance in terms of mechanical property recovery and self-healing efficiency.

6.3.2 Compression test

With this test, the compression behavior of cylindrical samples printed with formulations P1, P3, P5, and B5 was evaluated. Being a destructive test, where the samples at the end of the test are reduced to fragments, self-healing cycles were not conducted, but the state of the samples at the end of the test was qualitatively analyzed.

In *Figure 48*, the stress-strain curves of the various samples are reported, divided by formulation type. The samples printed with P5 and B5 resins exhibited brittle fracture behavior. P1 and P3, on the other hand, are characterized by plastic deformations, such that even reaching a displacement equal to the sample thickness minus 0.2 mm, they did not fragment when compressed. This result can be attributed to the mobility of the chains, an aspect more present in these formulations rather than in B5 or P5 due to the fact that borax is present in greater quantities.

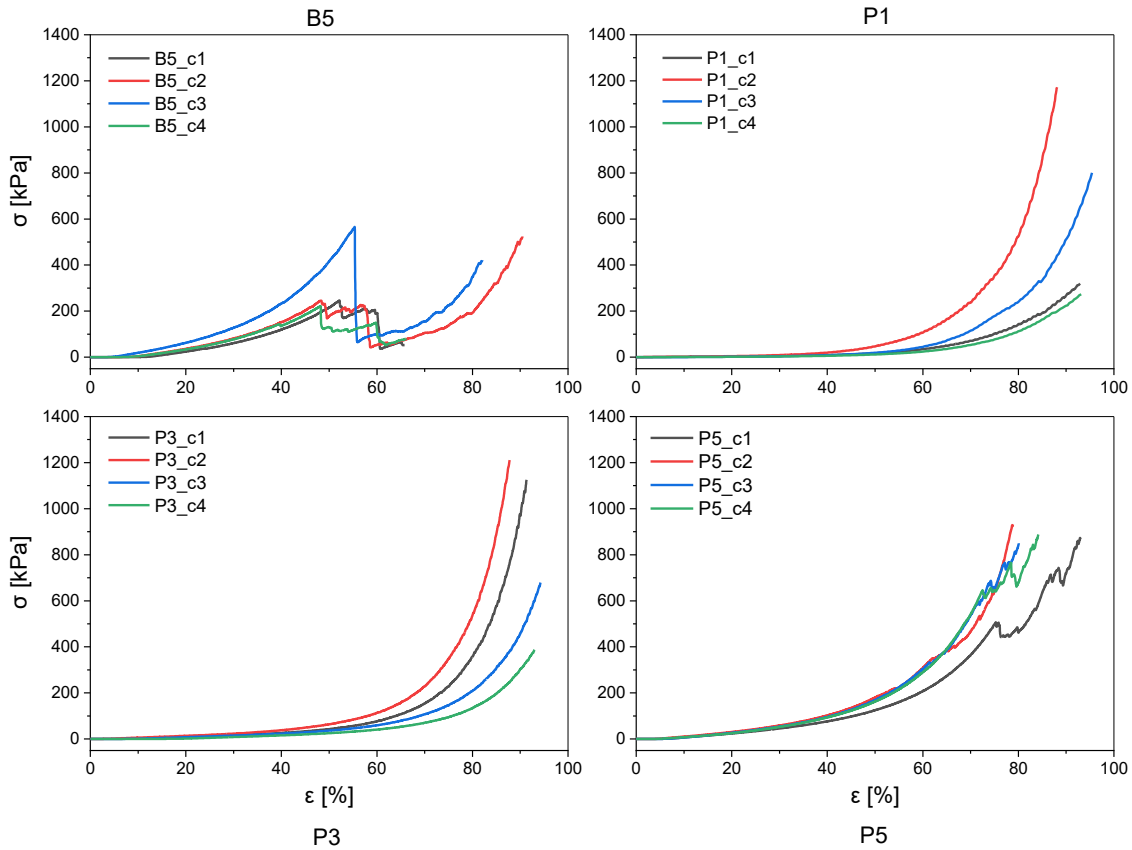


Figure 48. Stress-strain curves of the different formulations' samples obtained through compression test.

6.5 Evaluation of printability and resolution in DLP 3D printing

In this section, we evaluate the printability and resolution of Digital Light Processing (DLP) 3D printing by analysing the outcomes of the P3 formulation since it was the optimal formulation selected after the mechanical testing. Different 3D objects were mainly printed with this specific resin. Parameters such as exposure time, light intensity and layer thickness were optimized. Resin performances in terms of printing resolution and accuracy were assessed together with printing precision on edges, borders, and fillet.

Regarding P1, P5, and B5, their parameters and printing performance will be mentioned in order to compare them with those of P3, highlighting the printing needs that these resins have based on their composition.

It was decided to start with the printing parameters for P3, evaluating the results of material tests and rheology previously conducted. It was found that setting an exposure time of 35 seconds for the burn-in layers, 28 seconds for the remaining layers, and configuring a layer thickness of 70 μm yielded good printing results. The light intensity was set at 50 mW/cm^2 , the maximum of the printer.

In order to print dumbbell shaped specimens for tensile tests using various formulations, tests were conducted by printing with P5 using the same printing parameters as P3, which proved suitable. With these parameters, P5 can print objects characterized by a good degree of polymerization and precision. *Figure 49* shows a print of a 20x20x3mm honeycomb made using P5 resin.

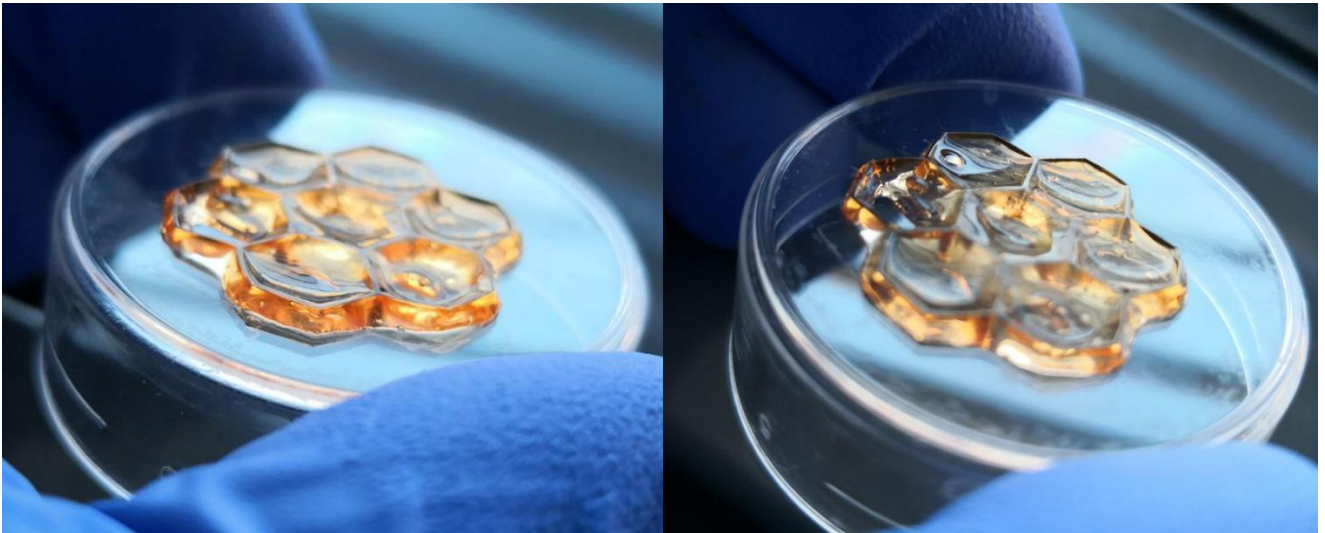


Figure 49. Honeycomb printed using P5 resin.

Printing precision appears fair for a hydrogel material: the structure present sharp edges and corners, However, it is also evident undesired polymerization out of the irradiated area, which implies lose of definition. On the other hand, this side effect can be minimized removing step by step the excess of resin on the part during the printing process.

In any case, applying the optimized parameters found for P3 formulation evan for P5, acceptable results were achieved.

Tests were also conducted with P1, using initially the same set of parameters as P3. With these, P1 samples result difficult to be printed, I good agreement with rheology results. This confirms that this formulation requires more time for polymerization. In *Figure 50*, a honeycomb based of P1 formulation printed employing P3 parameters is shown. As evident, the object's structure appears uneven. This is likely due to polymerization not effectively occurring at such low exposure times.



Figure 50. Result of a printed honeycomb using P1 resin with P3 printing parameters.

After some attempts, maintaining a layer thickness of 70 μm and a light intensity of 50 mW/cm^2 , good printing results were achieved by increasing the exposure times: 55 seconds for the burn-in layers and 45 seconds for the remaining layers. Printing with P1 is not advantageous as the printing times increase significantly.

Regarding B5, with the layer thickness and light intensity fixed, good printing can be achieved even at lower exposure times due to its high acrylic content and reactive nature. Specifically, exposure times of 28 seconds for the burn-in layers and 24 seconds for the remaining layers were set. With B5, therefore, we have reduced printing times compared to the P formulations. However, despite this advantage, B5 does not have self-healing capabilities.

The exposure times set for printing dumbbell shaped specimens of these four formulations are summarized in *Table 6*.

Regarding printing resolution, this was investigated by printing objects of various geometries using mainly P3 resin. Starting with the printing of a honeycomb, we can see in *Figure 51* that the printing resolution is good.

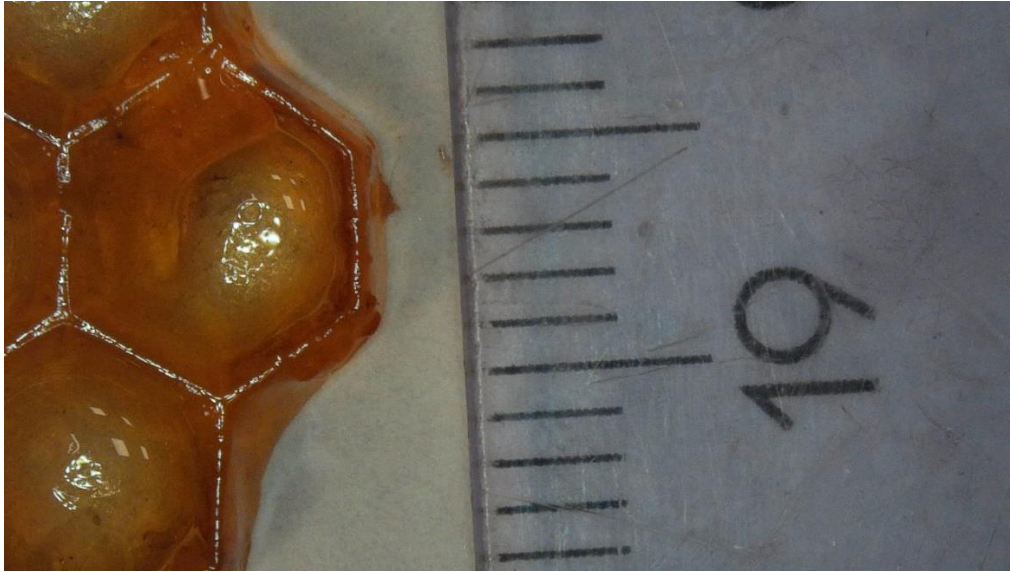


Figure 51. Honeycomb printed using P3 resin.

Furthermore, in *Figure 52*, it can be observed that there is also excellent printing precision on the edges and corners of the printed part.



Figure 52. Honeycomb printed using P3 resin.

To better evaluate spatial resolution, printing tests were conducted on benchmarks. The 3D model consists of a rectangular base with parallelepipeds designed in different thicknesses. *Figure 53* shows the printed benchmark, its dimensions are reported in *Table 14*.

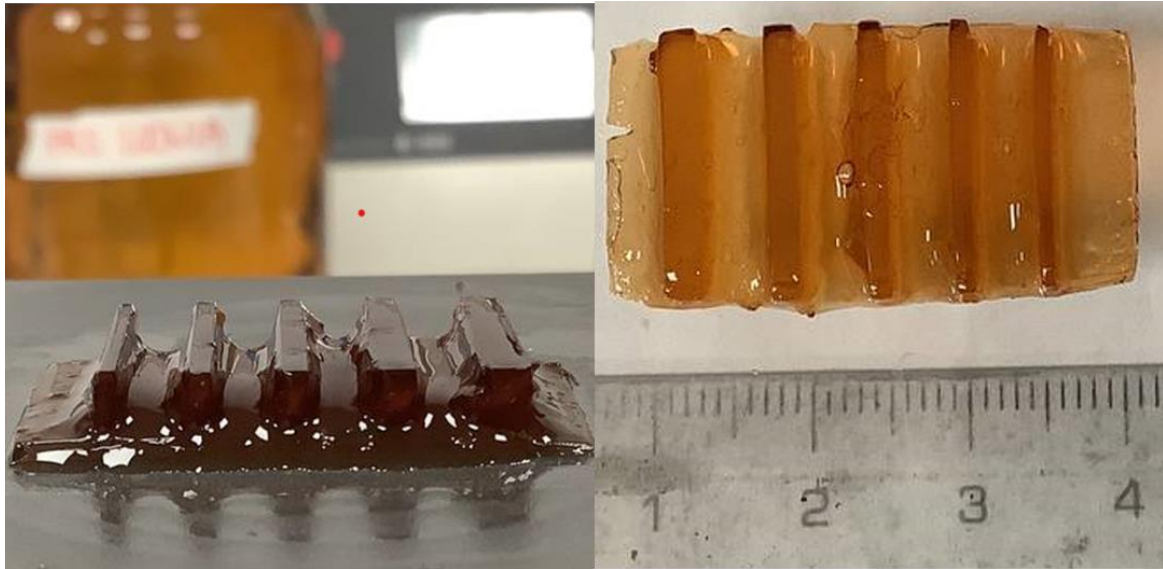


Figure 53. Benchmark 2,5 to 1 mm printed using P3 resin.

BASE HEIGHT	1,5 mm
PARELLELEPIPEDS HEIGHT	3,5 mm
THICKNESSES	2,5/2/1,5/1,3/1 mm

Table 14. Dimensions of the benchmark in Figure 52.

As can be seen, the printing on the horizontal plane features smooth surfaces and excellent precision. All five thicknesses were successfully printed. However, there is an issue with extra resin polymerizing on the vertical plane between the various parallelepipeds.

To explore if achieving even higher printing resolutions was possible, another benchmark with thinner thicknesses was printed. As shown in *Figure 54*, resolutions down to 250 μm were achieved.

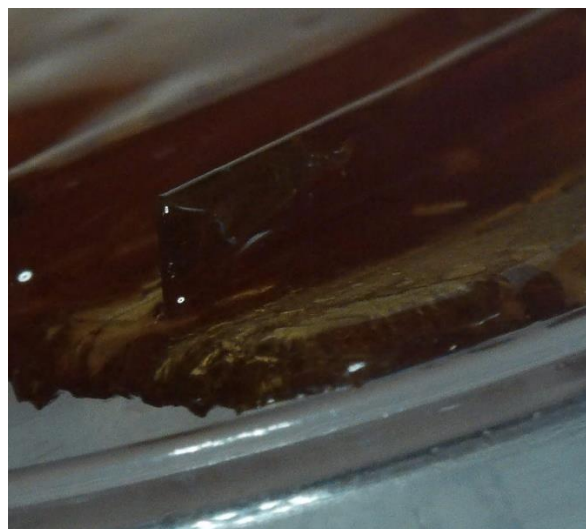


Figure 54. 0,25 mm thick parallelepiped printed using P3 resin.

In order to understand the resolution limits and overall capabilities of printing using P3 resin, an attempt was made to print a significantly more complex object. This object includes various geometrical shapes: parallelepipeds with thicknesses of 200 μm and 100 μm , triangular prisms, a cylinder, and two circular fillets. *Figure 55* shows the model printed in PLA.

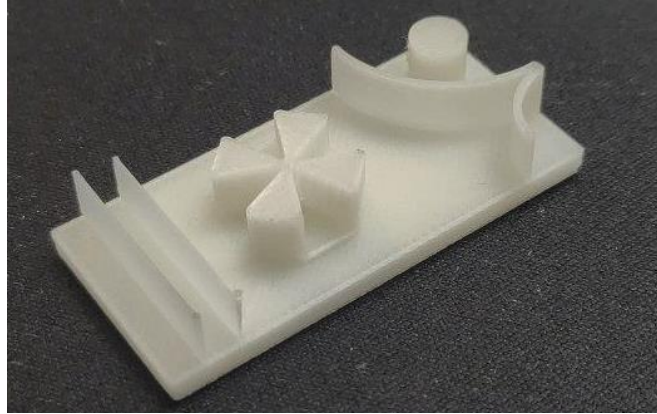


Figure 55. Multi-shape benchmark printed using PLA.

The printing result with P3 resin is shown in *Figure 56*.



Figure 56. Multi-shape benchmark printed using P3 resin.

The parallelepipeds could not be printed, indicating that at these thicknesses we are nearing the spatial resolution limit of the printer. Regarding the other parts, as mentioned earlier, there is good printing precision on the horizontal plane and overall accuracy in details. It can be seen that polymerization also occurs beyond the illuminated area due to resin diffusion on various parts during the printing phase (see fillets and triangular prisms). Given its geometric complexity and very small details, this is considered a good result for a hydrogel.

An attempt was made to print a 3D model of an agave leaf. This model features a distinctive geometry that includes suspended parts. *Figure 57* shows the 3D model and the printing result.

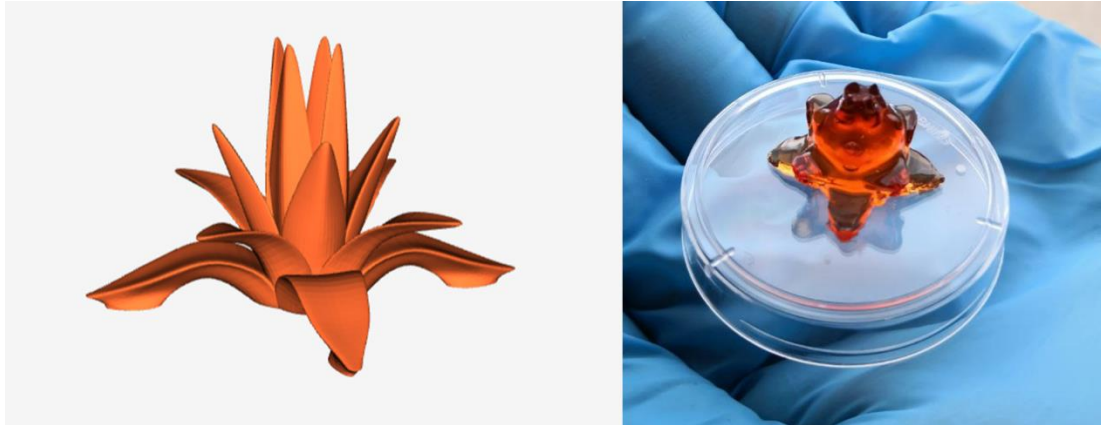


Figure 57. Agave leaf, 3D model and printed using P3 resin.

It can be noted that poor results were obtained with this model. This highlights that this resin is not well-suited for printing suspended parts.

Based on these results, it can be stated that using P3 resin allows for printing objects with a resolution of 250 μm and it has excellent printing precision on the horizontal plane, allowing for smooth surfaces and well-defined edges and corners. The main limitation in printing with this resin lies in its diffusion during printing, which can lead to undesired polymerizations and thus defects on the vertical plane.

6.6 Swelling test

In order to describe the water absorption capacity of this formulation, a swelling test was conducted on P3 formulation. In *Figure 58*, it can be seen that the P3 sample was able to absorb and retain water up to 7 times its dry weight.

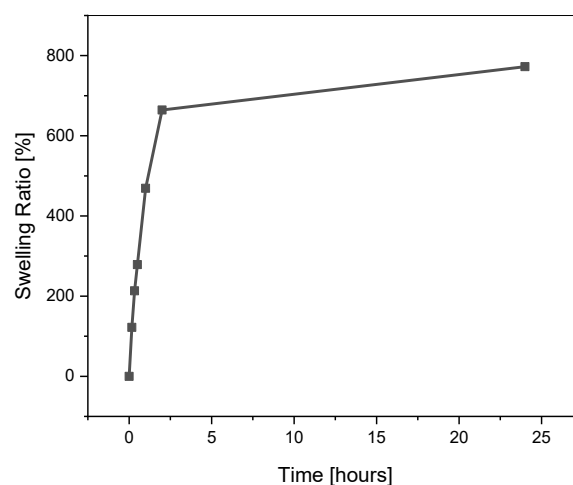


Figure 58. Results of swelling test on P3 cylindrical sample.

Given this result, the hydrogel has demonstrated excellent liquid retention capacity and could be useful for applications requiring this ability. Furthermore, after concluding the swelling test with the final measurement taken after 24 hours, the sample was left immersed in water for a week to assess its stability over an extended period. After seven days, the sample showed no structural degradation and remained manageable.

6.7 Qualitative self-healing test

To further evaluate self-healing, qualitative tests were conducted to assess the mechanical and visual recovery of samples. Rectangular samples were printed with P3 resin, and clean cuts were made using a razor blade. Subsequently, the two surfaces were repositioned as accurately as possible, and the samples were stored in sealed Petri dishes covered with Parafilm, along with dampened paper to prevent excessive drying. Typically, sample recovery was checked after three days, and generally, good results were obtained (see *Figure 59*).



Figure 59. P3 sample recovery after 3 days.

A crucial factor for the successful self-healing is the repositioning of the two parts of the sample. For effective self-healing, it is necessary to place the fractured surfaces in contact so that they adhere to each other as closely as possible.

7. Conclusion

In this thesis work, different formulations of photocurable resins for the fabrication of self-healing hydrogels via DLP 3D printing were characterized in order to find the optimal one in terms of self-healing efficiency, mechanical properties recovery and printability.

Using IR spectroscopy, we investigated the chemical composition of the hydrogel's elements and the final hydrogel, confirming that the resulting polymeric structure matched the intended composition for which it is possible to establish dynamic covalent bonds between the chains, enabling self-healing capabilities.

Through rheological and mechanical characterization methods we found the optimal formulation of the resin, identified as P3, which demonstrated excellent self-healing efficiency and a proper curing behaviour. Hydrogel samples printed with this specific resin were able to recover partially their mechanical properties after multiple cycles of self-healing. Mechanical tests demonstrated that P3 hydrogels could recover their mechanical features even after repeated self-healing processes and that its elastic modulus is appropriate for applications in tissue engineering such as cell growth support structures. Other resins also demonstrated some good mechanical properties, with P1 showing good ability in self-healing. However, among all, P3 proved to be the best based on mechanical recovery, self-healing efficiency and printability.

The printing process was optimized by selecting the best parameters for time of exposure, light intensity, and layer thickness, resulting in a controlled printing with good accuracy. Through the printing of various objects, it was possible to evaluate features of the printing process such as edge precision, corners, fillets, and spatial resolution.

Overall, the selected resin composition showed to be suitable for 3D printing of self-healing hydrogels via DLP technology. The findings of this study provide information for the development of advanced materials in tissue engineering and other biomedical applications. Future research could focus on further optimizing the resin formulation, exploring its long-term stability and conducting in vitro biocompatibility tests. Exploring additional applications and examining the scalability of the production process could pave the way for wider use of this self-healing hydrogels.

References

- [1] Geckil H, Xu F, Zhang X, Moon S, Demirci U. Engineering hydrogels as extracellular matrix mimics. *Nanomedicine (Lond)*. 2010 Apr;5(3):469-84. doi: 10.2217/nnm.10.12. PMID: 20394538; PMCID: PMC2892416.
- [2] Uematsu K, Hattori K, Ishimoto Y, Yamauchi J, Habata T, Takakura Y, Ohgushi H, Fukuchi T, Sato M. Cartilage regeneration using mesenchymal stem cells and a three-dimensional poly-lactic-glycolic acid (PLGA) scaffold. *Biomaterials*. 2005 Jul;26(20):4273-9. doi: 10.1016/j.biomaterials.2004.10.037. PMID: 15683651.
- [3] Boucard N, Viton C, Agay D, Mari E, Roger T, Chancerelle Y, Domard A. The use of physical hydrogels of chitosan for skin regeneration following third-degree burns. *Biomaterials*. 2007 Aug;28(24):3478-88. doi: 10.1016/j.biomaterials.2007.04.021. Epub 2007 Apr 19. PMID: 17482258.
- [4] Wang H, Heilshorn SC. Adaptable hydrogel networks with reversible linkages for tissue engineering. *Adv Mater*. 2015 Jul 1;27(25):3717-36. doi: 10.1002/adma.201501558. Epub 2015 May 19. PMID: 25989348; PMCID: PMC4528979.
- [5] Zhao L, Zhou Y, Zhang J, Liang H, Chen X, Tan H. Natural Polymer-Based Hydrogels: From Polymer to Biomedical Applications. *Pharmaceutics*. 2023 Oct 23;15(10):2514. doi: 10.3390/pharmaceutics15102514. PMID: 37896274; PMCID: PMC10610124.
- [6] Chen G, Sato T, Ushida T, Ochiai N, Tateishi T. Tissue engineering of cartilage using a hybrid scaffold of synthetic polymer and collagen. *Tissue Eng*. 2004 Mar-Apr;10(3-4):323-30. doi: 10.1089/107632704323061681. PMID: 15165449.
- [7] Christopher S. Brazel, Nikolaos A. Peppas, Pulsatile local delivery of thrombolytic and antithrombotic agents using poly(N-isopropylacrylamide-co-methacrylic acid) hydrogels, *Journal of Controlled Release*, Volume 39, Issue 1, 1996, Pages 57-64, ISSN 0168-3659, [https://doi.org/10.1016/0168-3659\(95\)00134-4](https://doi.org/10.1016/0168-3659(95)00134-4).
- [8] Kang Derwent JJ, Mieler WF. Thermo-responsive hydrogels as a new ocular drug delivery platform to the posterior segment of the eye. *Trans Am Ophthalmol Soc*. 2008;106:206-13; discussion 213-4. PMID: 19277236; PMCID: PMC2646442.
- [9] Rumon MMH, Akib AA, Sultana F, Moniruzzaman M, Niloy MS, Shakil MS, Roy CK. Self-Healing Hydrogels: Development, Biomedical Applications, and Challenges. *Polymers (Basel)*. 2022 Oct 26;14(21):4539. doi: 10.3390/polym14214539. PMID: 36365532; PMCID: PMC9654449.
- [10] Liu Y, Hsu SH. Synthesis and Biomedical Applications of Self-healing Hydrogels. *Front Chem*. 2018 Oct 2;6:449. doi: 10.3389/fchem.2018.00449. PMID: 30333970; PMCID: PMC6176467.
- [11] Li, Qiwen & Liu, Chenlu & Wen, Junru & Wu, Yongzhi & Shan, Yue & Liao, Jinfeng. (2017). The design, mechanism and biomedical application of self-healing hydrogels. *Chinese Chemical Letters*. 28. 10.1016/j.ccl.2017.05.007.
- [12] Li, Jinhua & Wu, Chengtie & Chu, Paul & Gelinsky, Michael. (2020). 3D printing of hydrogels: Rational design strategies and emerging biomedical applications. *Materials Science and Engineering: R: Reports*. 140. 100543. 10.1016/j.mser.2020.100543.

- [13] Arif, Zia Ullah & Khalid, Muhammad Yasir & Tariq, Ali & Hossain, Mokarram & Umer, Rehan. (2023). 3D printing of stimuli-responsive hydrogel materials: Literature review and emerging applications. *Giant*. 100209. 10.1016/j.giant.2023.100209.
- [14] Bagheri, Ali & Jin, Jianyong. (2019). Photopolymerization in 3D Printing. *ACS Applied Polymer Materials*. 1. 10.1021/acsapm.8b00165.
- [15] Zhang, Feng & Zhu, Liya & Li, Zongan & Wang, Shiyan & Shi, Jianping & Tang, Wenlai & Li, Na & Yang, Jiquan. (2021). The recent development of vat photopolymerization: A review. *Additive Manufacturing*. 48. 102423. 10.1016/j.addma.2021.102423.
- [16] Song, Chuhan & Zhao, Qian & Xie, Tao & Wu, Jingjun. (2024). DLP 3D printing of electrically conductive hybrid hydrogels via polymerization-induced phase separation and subsequent in situ assembly of polypyrrole. *Journal of Materials Chemistry A*. 12. 10.1039/D3TA06779C.
- [17] Caprioli M, Roppolo I, Chiappone A, Larush L, Pirri CF, Magdassi S. 3D-printed self-healing hydrogels via Digital Light Processing. *Nat Commun*. 2021 Apr 28;12(1):2462. doi: 10.1038/s41467-021-22802-z. PMID: 33911075; PMCID: PMC8080574.
- [18] Mercy, Lilly & Prakash, Subramanian. (2016). Self healing composite materials: A review. 9. 316-324.
- [19] Zhu W, Zhang J, Wei Z, Zhang B, Weng X. Advances and Progress in Self-Healing Hydrogel and Its Application in Regenerative Medicine. *Materials (Basel)*. 2023 Jan 31;16(3):1215. doi: 10.3390/ma16031215. PMID: 36770226; PMCID: PMC9920416.
- [20] Devi V K A, Shyam R, Palaniappan A, Jaiswal AK, Oh TH, Nathanael AJ. Self-Healing Hydrogels: Preparation, Mechanism and Advancement in Biomedical Applications. *Polymers (Basel)*. 2021 Oct 31;13(21):3782. doi: 10.3390/polym13213782. PMID: 34771338; PMCID: PMC8587783.
- [21] Dahlke, Jan & Zechel, Stefan & Hager, Martin & Schubert, Ulrich. (2018). How to Design a Self-Healing Polymer: General Concepts of Dynamic Covalent Bonds and Their Application for Intrinsic Healable Materials. *Advanced Materials Interfaces*. 5. 1800051. 10.1002/admi.201800051.
- [22] Basu S, Pacelli S, Paul A. Self-healing DNA-based injectable hydrogels with reversible covalent linkages for controlled drug delivery. *Acta Biomater*. 2020 Mar 15;105:159-169. doi: 10.1016/j.actbio.2020.01.021. Epub 2020 Jan 20. PMID: 31972367.
- [23] Zhang G, Lv L, Deng Y, Wang C. Self-Healing Gelatin Hydrogels Cross-Linked by Combining Multiple Hydrogen Bonding and Ionic Coordination. *Macromol Rapid Commun*. 2017 Jun;38(12). doi: 10.1002/marc.201700018. Epub 2017 May 8. PMID: 28481407.
- [24] Chen, Hao & Cheng, Ruoyu & Zhao, Xin & Zhang, Yuhui & Tam, Allison & Yan, Yufei & Shen, Haokai & Zhang, Y. Shrike & Qi, Jin & Feng, Yonghai & Liu, Lei & Pan, Guoqing & Cui, Wenguo & Deng, Lianfu. (2019). An injectable self-healing coordinative hydrogel with antibacterial and angiogenic properties for diabetic skin wound repair. *NPG Asia Materials*. 11. 10.1038/s41427-018-0103-9.
- [25] Wei Z, Yang JH, Du XJ, Xu F, Zrinyi M, Osada Y, Li F, Chen YM. Dextran-based self-healing hydrogels formed by reversible diels-alder reaction under physiological conditions. *Macromol Rapid Commun*. 2013 Sep;34(18):1464-70. doi: 10.1002/marc.201300494. Epub 2013 Aug 9. PMID: 23929621.

- [26] Chang R, Wang X, Li X, An H, Qin J. Self-Activated Healable Hydrogels with Reversible Temperature Responsiveness. *ACS Appl Mater Interfaces*. 2016 Sep 28;8(38):25544-51. doi: 10.1021/acsami.6b08279. Epub 2016 Sep 14. PMID: 27589014.
- [27] Cash, Jessica & Kubo, Tomohiro & Bapat, Abhijeet & Sumerlin, Brent. (2015). Room-Temperature Self-Healing Polymers Based on Dynamic-Covalent Boronic Esters. *Macromolecules*. 48. 10.1021/acs.macromol.5b00210.
- [28] He L, Szopinski D, Wu Y, Luinstra GA, Theato P. Toward Self-Healing Hydrogels Using One-Pot Thiol-Ene Click and Borax-Diol Chemistry. *ACS Macro Lett*. 2015 Jul 21;4(7):673-678. doi: 10.1021/acsmacrolett.5b00336. Epub 2015 Jun 10. PMID: 35596485.
- [29] Cromwell OR, Chung J, Guan Z. Malleable and Self-Healing Covalent Polymer Networks through Tunable Dynamic Boronic Ester Bonds. *J Am Chem Soc*. 2015 May 27;137(20):6492-5. doi: 10.1021/jacs.5b03551. Epub 2015 May 15. PMID: 25945818.
- [30] Luo F, Sun TL, Nakajima T, Kurokawa T, Zhao Y, Sato K, Ihsan AB, Li X, Guo H, Gong JP. Oppositely charged polyelectrolytes form tough, self-healing, and rebuildable hydrogels. *Adv Mater*. 2015 May 6;27(17):2722-7. doi: 10.1002/adma.201500140. Epub 2015 Mar 23. PMID: 25809867.
- [31] Yang, Ying & Urban, Marek. (2018). Self-Healing of Polymers via Supramolecular Chemistry. *Advanced Materials Interfaces*. 5. 1800384. 10.1002/admi.201800384.
- [32] Owusu-Nkwantabisah, Silas & Gillmor, Jeffrey & Switalski, Steven & Mis, Mark & Bennett, Grace & Moody, Roger & Antalek, Brian & Gutierrez, Robledo & Slater, Gary. (2017). Synergistic Thermoresponsive Optical Properties of a Composite Self-Healing Hydrogel. *Macromolecules*. 50. 10.1021/acs.macromol.7b00355.
- [33] Bilici, Çiğdem & Can, Volkan & Nöchel, Ulrich & Behl, Marc & Lendlein, Andreas & Okay, Oguz. (2016). Melt-Processable Shape-Memory Hydrogels with Self-Healing Ability of High Mechanical Strength. *Macromolecules*. 49. 7442-7449. 10.1021/acs.macromol.6b01539.
- [34] Nakahata M, Takashima Y, Harada A. Highly Flexible, Tough, and Self-Healing Supramolecular Polymeric Materials Using Host-Guest Interaction. *Macromol Rapid Commun*. 2016 Jan;37(1):86-92. doi: 10.1002/marc.201500473. Epub 2015 Sep 23. PMID: 26398922.
- [35] Zhang H, Xia H, Zhao Y. Poly(vinyl alcohol) Hydrogel Can Autonomously Self-Heal. *ACS Macro Lett*. 2012 Nov 20;1(11):1233-1236. doi: 10.1021/mz300451r. Epub 2012 Oct 9. PMID: 35607147.
- [36] Li G, Yan Q, Xia H, Zhao Y. Therapeutic-Ultrasound-Triggered Shape Memory of a Melamine-Enhanced Poly(vinyl alcohol) Physical Hydrogel. *ACS Appl Mater Interfaces*. 2015 Jun 10;7(22):12067-73. doi: 10.1021/acsami.5b02234. Epub 2015 May 29. PMID: 25985115.
- [37] Yuan, Le & Ren, Lijun & Tian, Xingtao & Huang, Zhiping & Xiao, YanHua & Wei, Sichen & Wang, Zhihua. (2016). Investigation on polyvinyl-alcohol-based rapidly gelling hydrogels for containment of hazardous chemicals. *RSC Adv*.. 6. 10.1039/C6RA14032G.
- [38] Chen, Lijun & Shao, Jia & Yu, Qijian & Wang, Sui. (2020). High-strength, anti-fatigue, stretchable self-healing polyvinyl alcohol hydrogel based on borate bonds and hydrogen bonds. *Journal of Dispersion Science and Technology*. 43. 1-14. 10.1080/01932691.2020.1844740.

- [39] Palmara G, Frascella F, Roppolo I, Chiappone A, Chiadò A. Functional 3D printing: Approaches and bioapplications. *Biosens Bioelectron.* 2021 Mar 1;175:112849. doi: 10.1016/j.bios.2020.112849. Epub 2020 Nov 24. PMID: 33250333.
- [40] Layani M, Wang X, Magdassi S. Novel Materials for 3D Printing by Photopolymerization. *Adv Mater.* 2018 Oct;30(41):e1706344. doi: 10.1002/adma.201706344. Epub 2018 May 13. PMID: 29756242.
- [41] Patel, Abhishek & Taufik, Mohammad. (2022). Extrusion-Based Technology in Additive Manufacturing: A Comprehensive Review. *Arabian Journal for Science and Engineering.* 49. 10.1007/s13369-022-07539-1.
- [42] Mostafaei, Amir & Elliott, Amy & Barnes, John & Cramer, Corson & Nandwana, Peeyush & Chmielus, Markus. (2020). Binder jet 3D printing – process parameters, materials, properties, and challenges. *Progress in Materials Science.* 100684. 10.1016/j.pmatsci.2020.100684.
- [43] Crivello, James & Reichmanis, Elsa. (2013). Photopolymer Materials and Processes for Advanced Technologies. *Chemistry of Materials.* 26. 533–548. 10.1021/cm402262g.
- [44] Zhang, Feng & Zhu, Liya & Li, Zongan & Wang, Shiyan & Shi, Jianping & Tang, Wenlai & Li, Na & Yang, Jiquan. (2021). The recent development of vat photopolymerization: A review. *Additive Manufacturing.* 48. 102423. 10.1016/j.addma.2021.102423.
- [45] Pagac, Marek & Hajnys, Jiri & Ma, Quoc-Phu & Jancar, Lukas & Jansa, Jan & Štefek, Petr & Mesicek, Jakub. (2021). A Review of Vat Photopolymerization Technology: Materials, Applications, Challenges, and Future Trends of 3D Printing. *Polymers.* 13. 598. 10.3390/polym13040598.
- [46] Kaur, Manmeet & Srivastava, Arun. (2002). Photopolymerization: A review. *JOURNAL OF MACROMOLECULAR SCIENCE Part C—Polymer Reviews Vol. C42. No. 4.* 481-512. 10.1081/MC-120015988.
- [47] Tomal W, Ortyl J. Water-Soluble Photoinitiators in Biomedical Applications. *Polymers (Basel).* 2020 May 7;12(5):1073. doi: 10.3390/polym12051073. PMID: 32392892; PMCID: PMC7285382.
- [48] Sun, Hong-Bo & Kawata, Satoshi. (2004). Two-Photon Photopolymerization and 3D Lithographic Microfabrication. 10.1007/b94405.
- [49] Kharkar PM, Rehmann MS, Skeens KM, Maverakis E, Kloxin AM. Thiol-ene click hydrogels for therapeutic delivery. *ACS Biomater Sci Eng.* 2016 Feb 8;2(2):165-179. doi: 10.1021/acsbiomaterials.5b00420. Epub 2016 Jan 11. PMID: 28361125; PMCID: PMC5369354.
- [50] Ouriques Machado, Thiago & Sayer, Claudia & Hermes de Araujo, Pedro Henrique. (2016). Thiol-ene polymerisation: A promising technique to obtain novel biomaterials. *European Polymer Journal.* 86. 10.1016/j.eurpolymj.2016.02.025.
- [51] Arslan, Mehmet & Gevrek, Tugce & Sanyal, Rana & Sanyal, Amitav. (2015). Fabrication of poly(ethylene glycol)-based cyclodextrin containing hydrogels via thiol-ene click reaction. *European Polymer Journal.* 62. 10.1016/j.eurpolymj.2014.08.018.
- [52] Wang K, Lu J, Yin R, Chen L, Du S, Jiang Y, Yu Q. Preparation and properties of cyclic acetal based biodegradable gel by thiol-ene photopolymerization. *Mater Sci Eng C Mater Biol Appl.*

2013 Apr 1;33(3):1261-6. doi: 10.1016/j.msec.2012.12.024. Epub 2012 Dec 9. PMID: 23827570.

- [53] Ooi HW, Mota C, Ten Cate AT, Calore A, Moroni L, Baker MB. Thiol-Ene Alginate Hydrogels as Versatile Bioinks for Bioprinting. *Biomacromolecules*. 2018 Aug 13;19(8):3390-3400. doi: 10.1021/acs.biomac.8b00696. Epub 2018 Jul 6. PMID: 29939754; PMCID: PMC6588269.
- [54] Fouassier, Jean & Lalevée, Jacques. (2012). Photoinitiators for Polymer Synthesis: Scope, Reactivity and Efficiency. 10.1002/9783527648245.
- [55] Salas, Alejandra & Zanatta, Marcileia & Sans, Victor & Roppolo, Ignazio. (2023). Chemistry in light-induced 3D printing. *ChemTexts*. 9. 10.1007/s40828-022-00176-z.
- [56] Lu H, Carioscia JA, Stansbury JW, Bowman CN. Investigations of step-growth thiol-ene polymerizations for novel dental restoratives. *Dent Mater*. 2005 Dec;21(12):1129-36. doi: 10.1016/j.dental.2005.04.001. Epub 2005 Jul 25. PMID: 16046231.10.1016/j.dental.2005.04.001. Epub 2005 Jul 25. PMID: 16046231.
- [57] Yongji He, Ning Li, Zuojia Xiang, Youjie Rong, Lisheng Zhu, Xiaobo Huang, Natural polyphenol as radical inhibitors used for DLP-based 3D printing of photosensitive gels, *Materials Today Communications*, Volume 33, 2022, 104698, ISSN 2352-4928, <https://doi.org/10.1016/j.mtcomm.2022.104698>.
- [58] Credi C, Fiorese A, Tironi M, Bernasconi R, Magagnin L, Levi M, Turri S. 3D Printing of Cantilever-Type Microstructures by Stereolithography of Ferromagnetic Photopolymers. *ACS Appl Mater Interfaces*. 2016 Oct 5;8(39):26332-26342. doi: 10.1021/acsami.6b08880. Epub 2016 Sep 20. PMID: 27610704.
- [59] 3D printing, IntechOpen, 2018. D. M. K. Christina Schmidleithner.
- [60] Haoyuan, Quan & Zhang, Ting & Xu, Hang & Luo, Shen & Nie, Jun & Zhu, Xiaoqun. (2020). Photo-curing 3D printing technique and its challenges. *Bioactive materials*. 5. 110-115. 10.1016/j.bioactmat.2019.12.003.
- [61] Gonzalez, Gustavo & Roppolo, Ignazio & Pirri, Candido & Chiappone, Annalisa. (2022). Current and emerging trends in polymeric 3D printed microfluidic devices. *Additive Manufacturing*. 55. 102867. 10.1016/j.addma.2022.102867.
- [62] Anandakrishnan, Nanditha. (2015). DESIGN AND OPTIMIZATION OF PEGDA AS A FUNCTIONAL MATERIAL FOR 3D PRINTING OF LIVER TISSUE.
- [63] Müller G, Zalibera M, Gescheidt G, Rosenthal A, Santiso-Quinones G, Dietliker K, Grützmacher H. Simple one-pot syntheses of water-soluble bis(acyl)phosphane oxide photoinitiators and their application in surfactant-free emulsion polymerization. *Macromol Rapid Commun*. 2015 Mar;36(6):553-7. doi: 10.1002/marc.201400743. Epub 2015 Feb 4. PMID: 25651079.
- [64] <https://www.asiga.com/max-x> [Online].
- [65] Rao, C. & Venkataraghavan, R. & Kasturi, T.. (2011). CONTRIBUTION TO THE INFRARED SPECTRA OF ORGANOSULPHUR COMPOUNDS. *Canadian Journal of Chemistry*. 42. 36-42. 10.1139/v64-006.
- [66] Neeti Goel, Nidhi Sinha, Binay Kumar, Growth and properties of sodium tetraborate decahydrate single crystals, *Materials Research Bulletin*, Volume 48, Issue 4, 2013, Pages 1632-1636, ISSN 0025-5408, <https://doi.org/10.1016/j.materresbull.2013.01.007>.

- [67] Smith, Merry & Northrop, Brian. (2014). Vibrational Properties of Boroxine Anhydride and Boronate Ester Materials: Model Systems for the Diagnostic Characterization of Covalent Organic Frameworks. *Chemistry of Materials*. 26. 3781–3795. 10.1021/cm5013679.
- [68] M. Imani, S. Sharifi, H. Mirzadeh, and F. Ziaee, "Monitoring of polyethylene glycol diacrylate-based hydrogel formation by real time NMR spectroscopy", *Iranian Polymer Journal (English Edition)*, vol. 16, no. 1, 2007.
- [69] Lu R, Gan W, Wu BH, Zhang Z, Guo Y, Wang HF. C-H stretching vibrations of methyl, methylene and methine groups at the vapor/alcohol (N = 1-8) interfaces. *J Phys Chem B*. 2005 Jul 28;109(29):14118-29. doi: 10.1021/jp051565q. PMID: 16852773.
- [70] Larkin, Peter. (2011). *Infrared and Raman Spectroscopy; Principles and Spectral Interpretation*. 10.1016/C2010-0-68479-3.